Subspace-based Mahalanobis damage detection robust to changes in excitation covariance

Szymon Gres, Michael Döhler, Palle Andersen, Laurent Mevel

Received: Added at production | Revised: Added at production | Accepted: Added at production

DOI: xxx/xxxx

RESEARCH ARTICLE

Subspace-based Mahalanobis damage detection robust to changes in excitation covariance

Szymon Greś[1] | Michael Döhler[2] | Palle Andersen[3] | Laurent Mevel[2]

[1]Aalborg University, Department of Civil and Structural Engineering, Aalborg, Denmark
[2]Univ. Gustave Eiffel, Inria, COSYS-SII, I4S Team, Rennes, France
[3]Structural Vibration Solutions A/S, Aalborg, Denmark

Correspondence
Szymon Greś, Aalborg University, Aalborg, Denmark. Email: sg@civil.aau.dk

Summary

In the context of detecting changes in structural systems, several vibration-based damage detection methods have been proposed and successfully applied to both mechanical and civil structures over the past years. These methods involve computing data-based features, which are then evaluated in statistical tests to detect damages. While being sensitive to damages, the data-based features are affected by changes in the ambient excitation properties that potentially lead to false alarms in the statistical tests, a characteristic that renders their use impractical for structural monitoring. In this paper, a damage detection method is presented that is robust to changes in the covariance of the ambient excitation. The proposed approach is based on the Mahalanobis distance of output covariance Hankel matrices, which are normalized with respect to possibly changing excitation properties. The statistical properties of the developed damage feature are reported, and used for efficient hypothesis testing. Its robustness towards changes in the excitation covariance is illustrated on numerical simulations and successfully tested on a numerical offshore foundation model.

KEYWORDS:
damage detection, ambient excitation, excitation changes, subspace-based methods, Mahalanobis distance

1 | INTRODUCTION

Vibration-based Structural Health Monitoring (SHM) refers to monitoring of the structural integrity based on measurements and sometimes a structural model. Different levels of damage diagnosis can be classified with a popular scheme of an increasing level of complexity namely, damage detection, localization, quantification and lifetime prediction[1]. These tasks can be addressed based on damage-sensitive features that are defined in the reference (healthy) state of the system, and which are evaluated for damage diagnosis during the operating states of the structure. Since the considered features are computed from vibration measurements, they may be affected by noise and changing environmental conditions, like variable temperature or excitation[2–4]. When not accounted for, those changes may lead to false alarms, a characteristic that impedes their application for structural monitoring. This paper investigates damage detection that is robust towards changes in the unknown ambient excitation covariance.

The evaluation of data-based damage features often relies on an outlier or novelty analysis[5–8], which is classically based on Mahalanobis distance[9–11], cointegration[12,13], whiteness tests[14], statistical process control[15] and other statistical hypothesis tests[16,17]. Damage features are e.g. based on modal parameters[3], Kalman filter innovations[14,18,19], wavelet transform[20,21], transmissibility functions[11,22,23], neural networks[24–27] and many other features from signal processing[28]. Reviews of the early developments of vibration-based damage detection can be found in[29–31]. The performance of these methods is conditioned on

several factors, e.g. the quality of parameters estimated from the data, the availability of large amount of training data from different damage scenarios[26], the ability to track the selected parameter estimates after identifying them from the healthy state of the structure[32] and the ability to account for changing environmental conditions like the temperature[4], amongst other factors.

In this context, methods that do not require (modal) parameter estimation on the test data and their tracking are particularly appealing. For such methods, damage-sensitive features are computed directly from the data using either empirical signal processing[21,27] or system theory-related[33] methods, and are then evaluated in statistical tests. For example, subspace-based damage detection[34–36] is a well-known statistical framework, with multiple applications to vibration-based SHM of e.g. bridges[37,38]. Its theoretical core is based on the asymptotic local approach for change detection[39], a statistical methodology used to detect changes by monitoring the mean of a parametrized Gaussian residual vector. In its data-driven premise, the subspace residual is inherently dependent on the natural changes of the ambient excitation, which poses a major challenge in its evaluation, since excitation conditions are in principle unknown and unmeasured. Therefore any important change therein may be falsely classified as a damage and raise false alarms. A solution to that problem lies in the design of a damage detection residual, whose mean value must be independent of such changes. This was for example achieved by a robust subspace residual relying on the singular value decomposition of the output covariance Hankel matrix[35], whose robustness was confirmed on experimental data[40]. A drawback of this approach is the assumption that the reference model is perfect, whereas in most applications it has to be estimated from data.

In this paper, a damage detection method is developed based on the Mahalanobis distance of Hankel matrices between reference and testing states of the system. The approach unites simplicity of the damage feature, robustness towards changing ambient excitation conditions by an appropriate normalization, and a sound statistical evaluation within the local approach framework. The aforementioned Mahalanobis distance[9] is widely used to assess the correspondence of a random variable to a given mean and variance, or of two different random variables. Some works have been devoted to variants of the Mahalanobis metric for varying variance conditions in different application domains[41–43]. Following their lines, several damage detection schemes that account for the covariance of the Hankel matrix computed in different states of the system, and normalize it by its covariance, are tested firstly in this paper. However, while performing well for simple changes in the excitation covariance, they are shown to be ineffective for general cases of excitation changes. Therefore a new data-driven residual is proposed, where the Hankel matrix is normalized by its stochastic part in the tested state with respect to possible excitation changes[44,45]. The statistical properties of the residual are evaluated to take into account uncertainties of both the reference and damaged states for an efficient damage detection test. The main outcome is that the test in the healthy state of the system does not depend on the excitation covariance, thus avoiding false alarms due to changing excitation properties.

This paper is organized as follows. Some background on vibration modeling and the considered problem of changing excitation properties is stated in Section 2. Different Mahalanobis distance-based metrics including simple normalizations with respect to excitation changes are illustrated in Section 3. The residual based on the normalized Hankel matrix difference is introduced in Section 4, and its statistical properties are evaluated for the development of a robust damage detection test. The application of the developed method on a large finite element model of an offshore foundation is enclosed in Section 5.

2 | BACKGROUND ON SYSTEM MODELING

In this section the dynamic model for output-only vibration data is introduced, and the impact of a change in the statistical properties of the ambient excitation on the output data is stated.

2.1 | Dynamic system models

The vibration behavior of the considered structure subject to unknown ambient excitation is assumed to be described by the differential equation

$$\mathcal{M}\ddot{z}(t) + C\dot{z}(t) + \mathcal{K}z(t) = f(t) \tag{1}$$

where t denotes continuous time, $\mathcal{M}, C, \mathcal{K} \in \mathbb{R}^{m\times m}$ are (usually unknown) mass, damping, and stiffness matrices, respectively, the vector $z(t) \in \mathbb{R}^m$ collects the displacements of the m degrees of freedom (DOF) of the structure, and $f(t) \in \mathbb{R}^m$ is the external unmeasured force. Observed at r sensor positions, e.g. by acceleration, velocity or displacement sensors at discrete time

instants $t = k\tau$ (with sampling rate $1/\tau$), system (1) can be transformed into the discrete-time state-space model[46]

$$\begin{cases} x_{k+1} = Ax_k + w_k \\ y_k = Cx_k + v_k \end{cases} \tag{2}$$

where $x_k \in \mathbb{R}^n$ are the states, $y_k \in \mathbb{R}^r$ are the outputs, vectors w_k and v_k denote the white process and output noise respectively, $A \in \mathbb{R}^{n\times n}$, $C \in \mathbb{R}^{r\times n}$ are the state and observation matrices, and $n = 2m$ is the model order. Let $R_i = \mathrm{E}(y_k y_{k-i}^T)$ be the theoretical output covariances of the measurements, which yield, following from (2), $R_i = CA^{i-1}G$, where $G = \mathrm{E}(x_{k+1} y_k^T)$ denotes the cross-covariance between the states and the outputs. The collection of R_i can be stacked to form a block Hankel matrix

$$\mathcal{H} = \begin{bmatrix} R_1 & R_2 & \dots & R_q \\ R_2 & R_3 & \dots & R_{q+1} \\ \vdots & \vdots & \ddots & \vdots \\ R_{p+1} & R_{p+2} & \dots & R_{p+q} \end{bmatrix} \in \mathbb{R}^{(p+1)r\times qr},$$

where p and q are chosen such that $\min(pr, qr) \geq n$ with often $p + 1 = q$. Matrix $\mathcal{H}$ enjoys the factorization property

$$\mathcal{H} = \mathcal{O}(C, A)\, \mathcal{C}(A, G), \tag{3}$$

where the observability and controllability matrices $\mathcal{O}(C, A)$ and $\mathcal{C}(A, G)$ are defined as

$$\mathcal{O}(C, A) = \begin{bmatrix} C \\ CA \\ \vdots \\ CA^p \end{bmatrix}, \quad \mathcal{C}(A, G) = \begin{bmatrix} G & AG & \dots & A^{q-1}G \end{bmatrix}. \tag{4}$$

Estimates $\hat{R}_i$ and consequently $\hat{\mathcal{H}}$ can be computed from the output covariances of the measurements $\{y_k\}_{k=1,\dots,N+p+q}$, e.g. by

$$\hat{\mathcal{H}} = \mathcal{Y}^+ \mathcal{Y}^{-T}, \tag{5}$$

where the data Hankel matrices $\mathcal{Y}^+$ and $\mathcal{Y}^-$ contain future and past time horizons

$$\mathcal{Y}^+ = \frac{1}{\sqrt{N}} \begin{bmatrix} y_{q+1} & y_{q+2} & \cdots & y_{N+q} \\ y_{q+2} & y_{q+3} & \cdots & y_{N+q+1} \\ \vdots & \vdots & \ddots & \vdots \\ y_{p+q+1} & y_{p+q+2} & \cdots & y_{p+q+N} \end{bmatrix}, \quad \mathcal{Y}^- = \frac{1}{\sqrt{N}} \begin{bmatrix} y_q & y_{q+1} & \cdots & y_{N+q-1} \\ y_{q-1} & y_q & \cdots & y_{N+q-2} \\ \vdots & \vdots & \ddots & \vdots \\ y_1 & y_2 & \cdots & y_N \end{bmatrix}.$$

Notice that matrices $\mathcal{O}(C, A)$ and $\mathcal{C}(A, G)$ can be obtained from a Singular Value Decomposition (SVD) of $\mathcal{H}$ thanks to factorization property (3), which is used for subspace-based system identification[47]. In consequence, the left part of the SVD of $\mathcal{H}$ contains information on the system matrices A and C, whereas the right part of the SVD is heavily dependent on the properties of the ambient excitation. In this work, the fact is exploited that the Hankel matrix – which is easily estimated from the measurement data – contains the dynamic properties of the system through matrices A and C, and thus can be used for monitoring changes therein.

2.2 | Change in the excitation properties

The influence of the process (excitation) and output noise properties on the state-space system (2) can be analyzed based on the properties of the forward stochastic model[48]. Define the covariance of the time-discrete ambient excitation $f_k = f(k\tau)$ related to model (1) as $Q = \mathrm{E}(f_k f_k^T)$. Since no assumptions are required on the spatial independence of the excitation, Q is in general a full matrix, which is positive semi-definite. Define the noise covariance matrices related to model (2) as

$$\mathrm{E}\left(\begin{bmatrix} w_k \\ v_k \end{bmatrix} \begin{bmatrix} w_l & v_l \end{bmatrix} \right) = \begin{bmatrix} \tilde{Q} & S \\ S^T & R \end{bmatrix} \delta_{kl}, \quad \text{where} \quad \tilde{Q} = \begin{bmatrix} 0 & 0 \\ 0 & \mathcal{M}^{-1} Q \mathcal{M}^{-T} \end{bmatrix},$$

and $\delta_{kl} = 1$ iff $k = l$ and zero otherwise. Then, it holds[48]

$$\mathrm{E}(x_k\, x_k^T) = \Sigma_s = A\Sigma_s A^T + \tilde{Q} \tag{6}$$

$$\mathrm{E}(y_k\, y_k^T) = R_0 = C\Sigma_s C^T + R \tag{7}$$

$$\mathrm{E}(x_{k+1}\, y_k^T) = G = A\Sigma_s C^T + S \tag{8}$$

A variation in the ambient excitation covariance Q results in a change in the process noise covariance $\tilde{Q}$, which affects the Lyapunov equation for state covariance (6) that both modifies the covariance between the measurements (7) and covariance between measurements and the states G in (8). This leads to changes in the right part in the factorization (4) of the Hankel matrix when built on measurement from varying conditions, since this part depends on G. Therefore a data-driven damage detection test employing data sets from different excitation conditions should appreciate a change in the process noise covariance by using robust features or adopting a proper normalization scheme.

3 | MAHALANOBIS DISTANCE ON HANKEL MATRICES FOR DAMAGE DETECTION

Based on features extracted from measurement data in the reference and in the current test state, the goal of damage detection is to evaluate whether there is a significant change between both states or not. In this paper, the problem of possibly changing excitation properties between both states is considered for the definition of the feature and the damage detection metric. This problem is illustrated in the context of different empirical Mahalanobis distance-based damage detection metrics on a simple numerical example in the following.

The Mahalanobis distance is a measure of the distance between a point P and a distribution D, introduced by P. C. Mahalanobis in 1936[9]. This distance is zero if P is at the mean of D, otherwise it is equal to the number of standard deviations from P to the mean of D. It is considered as a dissimilarity measure between two random vectors $\vec{x}$ and $\vec{y}$ of the same distribution with the covariance matrix Σ

$$d(\vec{x}, \vec{y}) = \sqrt{(\vec{x} - \vec{y})^T \Sigma^{-1} (\vec{x} - \vec{y})}. \tag{9}$$

In the Gaussian case, it is well-known that if $\vec{y}$ is constant and equal to the mean of $\vec{x}$, then d^2 is χ^2 distributed[49]. More difficult, however, is the analysis of d^2 when $\vec{y}$ is Gaussian, from the same or a different distribution. Furthermore, when the variances of $\vec{x}$ and $\vec{y}$ are different, the distance d^2 can be large. Thus, analyzing the distribution and statistical properties of d^2 can be troublesome. In this paper, the Mahalanobis distance is defined based on the difference between vectorized output covariance Hankel matrices, that are computed from the structural response measurements in a reference and a test state. These Hankel matrices are straightforwardly computed from the measurement data and contain the dynamic system information that is sensitive to structural damages. As such, they are good candidates for a damage-sensitive feature that does not need the identification of modal parameters and their tracking.

As a result the analyzed distance d^2 inherits the properties of the Hankel matrices and the related output covariance sequences. The properties of the output covariances are inherently affected by properties of the ambient excitation, which is illustrated in this section. The underlying statistical analysis of d^2 is valid asymptotically for a large number of samples, which is appropriate for damage detection in practice when long data sets of the response measurements are collected from operating structures.

3.1 | Numerical example

In this section, a numerical experiment is defined for illustration and validation of the investigated damage detection methods throughout the paper. The studied case is a 6 DOF chain-like system that, for any consistent set of units, is modeled with spring stiffness $k_1 = k_3 = k_5 = 100$ and $k_2 = k_4 = k_6 = 200$, mass $m_i = 1/20$ and a proportional damping matrix such that all modes have a damping ratio of 3%. Its illustration is presented on Figure 1 and the exact modal parameters of the system are depicted in Table 1. The system is excited by a white noise signal with some excitation covariance Q and acting at all DOFs. The structural accelerations are simulated at DOFs 1, 3 and 5 at a sampling frequency of 50 Hz, and Gaussian white measurement noise with

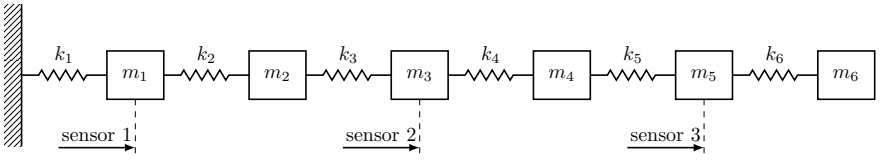

FIGURE 1 Illustration of 6 DOF chain system used for numerical evaluation of different approaches for damage detection.

5% of the standard deviation of the output is added to the each response measurement. Damage is modeled as a gradual stiffness reduction of the second spring, first by reducing k_2 by 5% and second by 10%.

The simulation campaign consists of a reference built with data length $N_0 = 2{,}000{,}000$, and several tested states each simulated with data length $N = 100{,}000$. Different excitation covariance scenarios are considered, namely first a base-case, where Q is the identity matrix I_6, second where every excitation point is scaled with a scalar constant a such that $Q = a \cdot I_6$, and last where Q is not a diagonal matrix, but a full, positive definite matrix that is randomly computed as $Q = bb^T$ where $b \in \mathbb{R}^{6\times 6}$ is a matrix whose entries are drawn from a standard normal distribution. Each data set of the test states corresponds to the healthy state or different damage levels, each for the different excitation scenarios.

3.2 | Damage detection based on difference of Hankel matrices

Since the Hankel matrix contains the dynamic properties of the system, a change therein may indicate damage and thus the Mahalanobis distance can be used to evaluate it. Let $\hat{\mathcal{H}}_{\text{ref}}$ and $\hat{\mathcal{H}}_{\text{test}}$ be the estimates of the Hankel matrices from the reference and tested states, respectively, and let their associated covariance matrices be $\Sigma_{\hat{\mathcal{H}}_{\text{ref}}} = \text{cov}(\text{vec}(\hat{\mathcal{H}}_{\text{ref}}))$ and $\Sigma_{\hat{\mathcal{H}}_{\text{test}}} = \text{cov}(\text{vec}(\hat{\mathcal{H}}_{\text{test}}))$, where $\text{vec}(\cdot)$ denotes the column stacking vectorization operator.

The classical Mahalanobis distance formulation (9) writes for the Hankel matrices as

$$d_1(\hat{\mathcal{H}}_{\text{ref}}, \hat{\mathcal{H}}_{\text{test}}) = \sqrt{\text{vec}(\hat{\mathcal{H}}_{\text{ref}} - \hat{\mathcal{H}}_{\text{test}})^T \Sigma^{-1}_{\hat{\mathcal{H}}_{\text{ref}}} \text{vec}(\hat{\mathcal{H}}_{\text{ref}} - \hat{\mathcal{H}}_{\text{test}})}, \tag{10}$$

involving the covariance computed on the reference data set. However, not only changes in the dynamic properties but also changes in the ambient excitation covariance Q have an influence on the output covariances, and thus on $\hat{\mathcal{H}}_{\text{test}}$ and the distance d_1, as explained in Section 2.2. Therefore, changes in Q between the reference and test data could be counteracted by a normalization taking into account the covariance related to both $\hat{\mathcal{H}}_{\text{ref}}$ and $\hat{\mathcal{H}}_{\text{test}}$, or by directly normalizing the autocovariance of the data. The resulting simple normalization strategies are reflected in the following distance formulations.

Taking into account the covariance related both to the reference and the test data[41] after a change in Q leads to

$$d_2(\hat{\mathcal{H}}_{\text{ref}}, \hat{\mathcal{H}}_{\text{test}}) = \sqrt{\text{vec}(\hat{\mathcal{H}}_{\text{ref}} - \hat{\mathcal{H}}_{\text{test}})^T \Sigma^{-1}_{\hat{\mathcal{H}}} \text{vec}(\hat{\mathcal{H}}_{\text{ref}} - \hat{\mathcal{H}}_{\text{test}})}\,, \tag{11}$$

where $\Sigma_{\hat{\mathcal{H}}} = \Sigma_{\hat{\mathcal{H}}_{\text{ref}}} + \Sigma_{\hat{\mathcal{H}}_{\text{test}}}$. Next, the output data themselves can be normalized with respect to the standard deviation of each channel[43], or altogether by their autocovariance matrix R_0 (see (7)), taking also into account the correlation between different channels. This leads to

$$d_3(\hat{\mathcal{H}}_{\text{ref}}, \hat{\mathcal{H}}_{\text{test}}) = \sqrt{\text{vec}(\hat{\mathcal{H}}^W_{\text{ref}} - \hat{\mathcal{H}}^W_{\text{test}})^T \Sigma^{-1}_{\hat{\mathcal{H}}^W_{\text{ref}}} \text{vec}(\hat{\mathcal{H}}^W_{\text{ref}} - \hat{\mathcal{H}}^W_{\text{test}})} \tag{12}$$

where $\hat{\mathcal{H}}^W = W_1^{-1} \hat{\mathcal{H}} W_2^{-1}$ with $W_1 = I_{p+1} \otimes \hat{R}_0^{1/2}$ and $W_2 = I_q \otimes \hat{R}_0^{1/2}$, where $\otimes$ denotes the Kronecker product. Finally, taking into account the covariances of both data sets in this setting is tested in the distance

$$d_4(\hat{\mathcal{H}}_{\text{ref}}, \hat{\mathcal{H}}_{\text{test}}) = \sqrt{\text{vec}(\hat{\mathcal{H}}^W_{\text{ref}} - \hat{\mathcal{H}}^W_{\text{test}})^T \Sigma^{-1}_{\hat{\mathcal{H}}^W} \text{vec}(\hat{\mathcal{H}}^W_{\text{ref}} - \hat{\mathcal{H}}^W_{\text{test}})}, \tag{13}$$

where $\Sigma_{\hat{\mathcal{H}}^W} = \Sigma_{\hat{\mathcal{H}}^W_{\text{ref}}} + \Sigma_{\hat{\mathcal{H}}^W_{\text{test}}}$ accounts for the uncertainty in both tested and reference data sets.

3.3 | Evaluation of empirical methods

The distances presented above are tested on the numerical validation example from Section 3.1, where the impact of changing excitation is evaluated for different cases of simple and more complex excitation covariance matrices in the healthy and damaged states. The results are depicted in Figures 2–5 for the respective distance metrics d_1–d_4 defined in (10)–(13). In each example

TABLE 1 Exact modal parameters of the chain system.

Mode	1	2	3	4	5	6
Natural frequency f_i (Hz)	1.936	5.618	8.682	14.494	15.798	17.007
Damping ratio ζ_i (%)	3	3	3	3	3	3

multiple data sets in the reference state are simulated with a constant excitation covariance of $Q = I$, on which the above distances are computed. Then, further healthy data sets are simulated in the reference state as well as data sets in both damaged states for different choices of Q. Distance values that are significantly higher than those of the reference state would indicate damage.

Firstly a simple scaling of Q is tested. The performance of the classical Mahalanobis distances d_1 and d_2, computed either with Σ in the reference or current state, is good when the noise properties are kept constant, which is expected, as seen in Figures 2 (left) and 3 (left). However, the classical Mahalanobis distance fails to detect damages or exhibits false alarms even under simple changes in the excitation covariance, as seen in Figures 2 (right) and 3 (right).

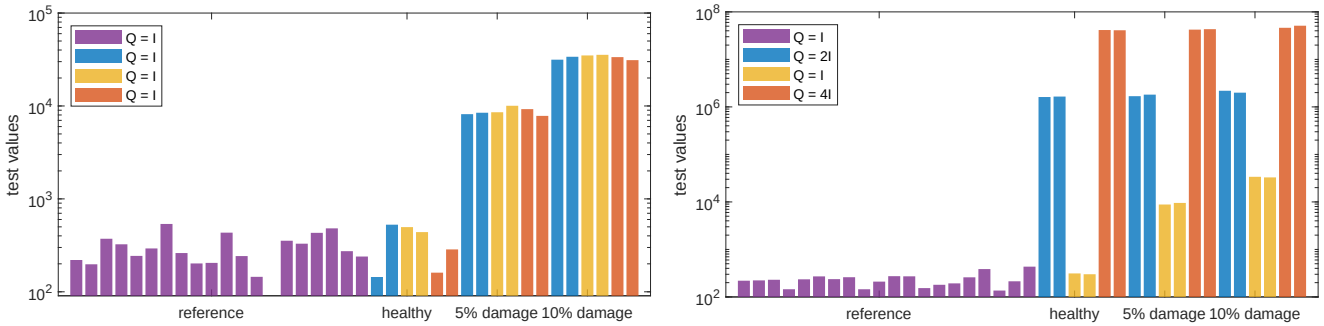

FIGURE 2 Damage detection under simple excitation covariances with d_1, using unnormalized Hankel matrices and covariance computed in the reference state.

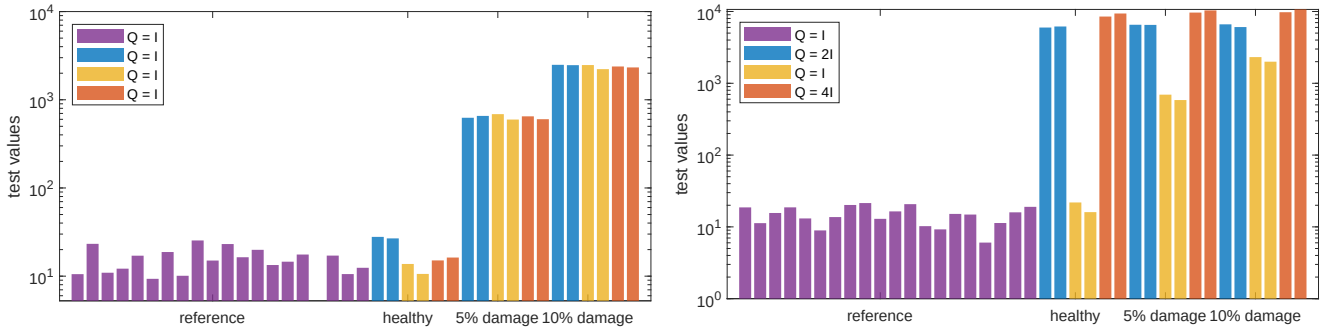

FIGURE 3 Damage detection under simple excitation covariances with d_2, using unnormalized Hankel matrices and covariance computed from both reference and tested data sets.

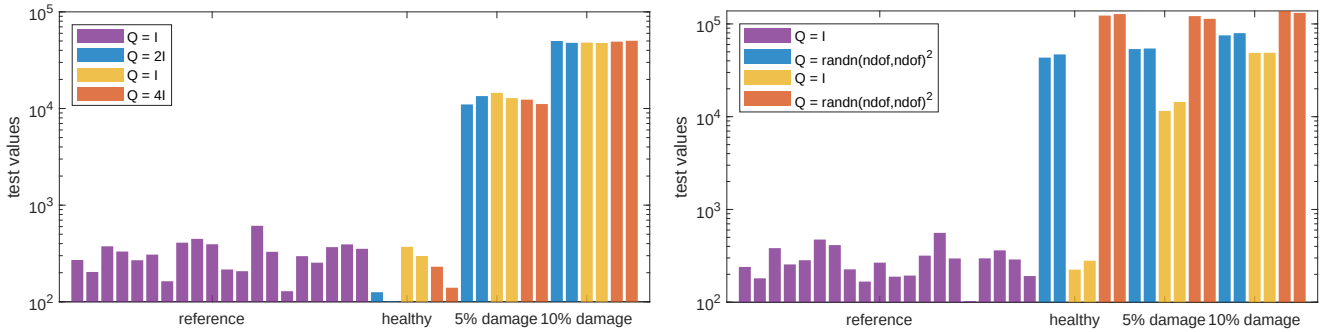

FIGURE 4 Damage detection with simple (left) and complex (right) excitation covariances with d_3, using Hankel matrices normalized by R_0 and covariance computed in the reference state.

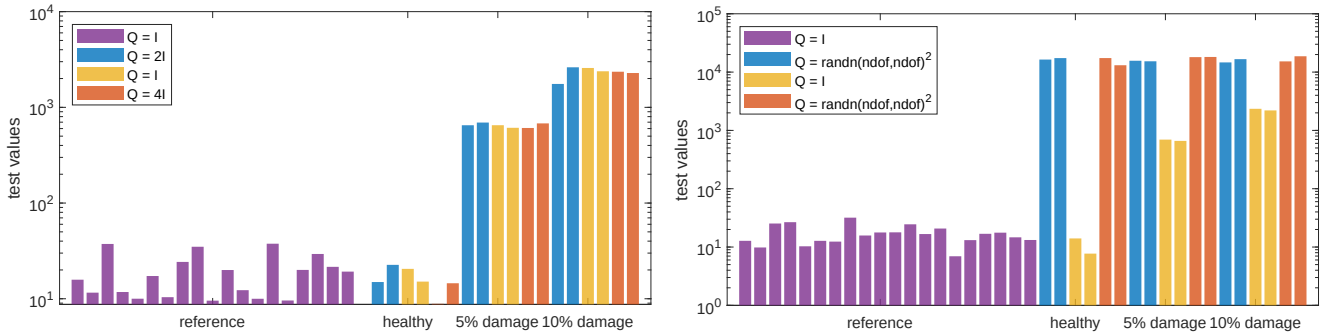

FIGURE 5 Damage detection with simple (left) and complex (right) excitation covariances with d_4, using Hankel matrices normalized by R_0 Hankel matrices and covariance including both the reference and tested states.

An empirical attempt to compensate for such covariance changes consists in the normalization of the measurements by R_0 as proposed in the d_3 metric in (12). The results from this scheme are depicted in Figure 4. As illustrated in Figure 4 (left), a simple scaling of the excitation covariance can be handled, whereas more complex Q matrices lead to false alarms and bad performance for the detection in Figure 4 (right), where no separation between healthy and damaged states is possible. One possible strategy to resolve this is to account for the covariance of both metrics in reference and tested states as proposed in the d_4 metric, depicted in Figure 5. However, the considered scheme is not invariant towards more complex excitation changes either, despite the normalization and taking into account the covariance of both Hankel matrices.

These results show that the proposed simple normalization schemes are insufficient for defining a distance metric for damage detection that is robust towards changes in the excitation covariance. In particular, none of them is able to avoid false alarms in the reference state, nor a clear separation between values of the healthy and damaged states is possible. Moreover, none of these approaches, being empirical, benefit of a theoretical background allowing to infer a statistical behavior of the considered metrics. Consequently, a threshold for alarms and decision whether the structure is being damaged or not cannot be established. These points will be addressed with the approach of this paper that is developed in the next section.

4 | DAMAGE DETECTION WITH NORMALIZATION TOWARDS CHANGES IN THE EXCITATION COVARIANCE

In this section a new damage detection residual based on the Hankel matrix difference is introduced. Hereby, the structure of the Hankel matrices is further explored to achieve robustness towards changes in the excitation covariance, for which the simple normalization approaches from the previous section were insufficient. The proposed residual is purely data-based, thus can be applied directly on the structural response measurements and no structural model is required to evaluate it. The possible changes in the excitation covariance are taken into account by employing a theoretically sound normalization scheme. It is shown that the newly developed metric fits into the well-known asymptotic local approach to change detection [34,35,39] framework. Therein, the residual is shown to be asymptotically Gaussian, and its mean changes between the healthy and damaged states. This paper outlines the schemes to evaluate the mean and the covariance of the proposed residual. A hypothesis test to distinguish between healthy and damaged states is developed, whose formulation resembles a Mahalanobis distance. The test statistics is asymptotically χ^2 distributed, and its mean is shown to be robust to changes in the excitation covariance in the healthy state, thus in particular avoiding false alarms due to excitation changes.

4.1 | Normalization scheme

Potential changes in the excitation covariances Q_{ref} and Q_{test} between reference and tested states need to be considered when comparing the Hankel matrix estimates $\hat{\mathcal{H}}_{\text{ref}}$ and $\hat{\mathcal{H}}_{\text{test}}$ for damage detection. Indeed, a change in the excitation covariance induces changes in the Hankel matrix independently from damage, as pointed out in Section 2.2 and illustrated in the previous section. The analysis of these changes and the development of their normalization is made based on the theoretical Hankel matrices $\mathcal{H}_{\text{ref}}$ and $\mathcal{H}_{\text{test}}$, which are the limits of the estimates.

Each Hankel matrix of output covariances has the factorization property (3) into the observability matrix $\mathcal{O}(C, A)$ and controllability matrix $\mathcal{C}(A, G)$ defined in (4). While the left factor $\mathcal{O}(C, A)$ depends on the system dynamics and thus is sensitive to damages, the right factor $\mathcal{C}(A, G)$ depends in particular on the cross-covariance G that itself is a function of the excitation covariance. The idea behind the normalization is to replace the right factor of the Hankel matrix in the tested state (corresponding to Q_{test}) with the one of the reference state (corresponding to Q_{ref}). Then, the normalized test Hankel matrix is comparable to the reference matrix regarding the excitation, while the left damage-sensitive part of the factorization remains unchanged.

To develop such a normalization scheme, consider first the case when both matrices $\mathcal{H}_{\text{ref}}$ and $\mathcal{H}_{\text{test}}$ correspond to the system in the healthy state, before it is applied to the general case in the next section. Then, these Hankel matrices can be factorized as $\mathcal{H}_{\text{ref}} = \mathcal{O}(C, A)\mathcal{C}(A, G_{\text{ref}})$ and $\mathcal{H}_{\text{test}} = \mathcal{O}(C, A)\mathcal{C}(A, G_{\text{test}})$ (see (3)). These factorizations, however, are not unique and yield factors in arbitrary state space bases[44,45]. Hence, the right parts of the individual factorizations of $\mathcal{H}_{\text{ref}}$ and $\mathcal{H}_{\text{test}}$ cannot be simply replaced. A solution to this problem is based on the simultaneous factorization of the juxtaposed matrices, which satisfies

$$\begin{bmatrix}\mathcal{H}_{\text{ref}} & \mathcal{H}_{\text{test}}\end{bmatrix} = \mathcal{O}(C, A)\begin{bmatrix}\mathcal{C}(A, G_{\text{ref}}) & \mathcal{C}(A, G_{\text{test}})\end{bmatrix}, \tag{14}$$

and where the same basis of the factors is enforced. Then, the excitation normalization of the Hankel matrix in the tested state can be carried out by replacing its right factor with the one of the reference state, corresponding to the product

$$\mathcal{H}_{\text{test}}\,\mathcal{C}(A, G_{\text{test}})^{\dagger}\,\mathcal{C}(A, G_{\text{ref}}), \tag{15}$$

which now has the same excitation properties as $\mathcal{H}_{\text{ref}}$. For a computational realization of this normalization, the involved factors can be obtained by means of the SVD as follows. The SVD of the juxtaposed Hankel matrices (14) yields

$$\begin{bmatrix}\mathcal{H}_{\text{ref}} & \mathcal{H}_{\text{test}}\end{bmatrix} = \begin{bmatrix}U_{\text{s}} & U_{\text{ker}}\end{bmatrix}\begin{bmatrix}D_{\text{s}} & 0\\ 0 & 0\end{bmatrix}\begin{bmatrix}V_{\text{s}}^T\\ V_{\text{ker}}^T\end{bmatrix} = U_{\text{s}}\begin{bmatrix}\mathcal{Z}_{\text{ref}} & \mathcal{Z}_{\text{test}}\end{bmatrix}, \tag{16}$$

where $\operatorname{rank}\left(\begin{bmatrix}\mathcal{H}_{\text{ref}} & \mathcal{H}_{\text{test}}\end{bmatrix}\right) = n$, $U_{\text{s}} \in \mathbb{R}^{(p+1)r\times n}$ contains the left singular vectors, $D_{\text{s}} \in \mathbb{R}^{n\times n}$ contains the non-zero singular values and $V_{\text{s}} \in \mathbb{R}^{2qr\times n}$ contains the right singular vectors that are split into $V_{\text{s}}^T = \begin{bmatrix}V_{\text{s,ref}}^T & V_{\text{s,test}}^T\end{bmatrix}$ corresponding to $\mathcal{H}_{\text{ref}}$ and $\mathcal{H}_{\text{test}}$ respectively, and the right factors are

$$\mathcal{Z}_{\text{ref}} = D_{\text{s}}V_{\text{s,ref}}^T, \quad \mathcal{Z}_{\text{test}} = D_{\text{s}}V_{\text{s,test}}^T. \tag{17}$$

Then, the desired normalization (15) of the Hankel matrix in the tested state is obtained as

$$\mathcal{H}_{\text{test}}\mathcal{Z}_{\text{test}}^{\dagger}\mathcal{Z}_{\text{ref}}, \tag{18}$$

which shares the same stochastic controllability matrix and hence excitation properties as $\mathcal{H}_{\text{ref}}$. With this normalization, a residual for damage detection robust to changes in the excitation covariance is built based on the difference between the Hankel matrix in the reference state and the normalized Hankel matrix in the tested state, which is described in the following section.

4.2 | Residual definition

For the definition of the damage detection residual based on a normalized Hankel matrix difference, a system parameter is formalized first to define healthy and damaged states. Damage in the system is related to a change in some dynamic system parameters, such as modal parameters or physical parameters that are directly related to the structural elements. A change in those system parameters is then reflected in the measurement data, on which the residual is computed. Let θ denote such a parametrization of the structural properties of the considered system, and let θ_* be its value in the healthy state[50]. Note that neither θ_* nor θ need to be known for a non-parametric evaluation of the residual. In this case θ_* and θ simply refer to the healthy and current tested state of the structure, respectively.

Measurement data $\{y_k\}$ is obtained from the system in the healthy state under θ_*, and from the unknown tested state under (unknown) parameter θ. In both states, the Hankel matrix estimates $\hat{\mathcal{H}}_{\text{ref}}^{\theta_*}$ and $\hat{\mathcal{H}}_{\text{test}}^{\theta}$ are obtained from data sets of lengths M and N, respectively. They are estimates of the exact Hankel matrices $\mathcal{H}_{\text{ref}}^{\theta_*}$ and $\mathcal{H}_{\text{test}}^{\theta}$ under possibly different excitation covariances Q_{ref} and Q_{test}.

In order to compare the measurements from healthy and tested states, a residual is expressed that takes into account possible excitation changes. First, consider the case when $\theta = \theta_*$, i.e. when the system is in the healthy state as in the previous section. Then, it follows from (16)

$$\mathcal{H}_{\text{test}}^{\theta}\mathcal{Z}_{\text{test}}^{\dagger}\mathcal{Z}_{\text{ref}} - \mathcal{H}_{\text{ref}}^{\theta_*} = 0 \quad \text{if} \quad \theta = \theta_*, \tag{19}$$

which is the characteristic property that is required for defining a residual with mean zero in the healthy state. Next, consider the case when $\theta \neq \theta_*$, i.e. when the system is damaged. Then, defining $\mathcal{Z}_{\text{ref}}$ and $\mathcal{Z}_{\text{test}}$ as in (17) from the SVD (16) of the juxtaposed matrices $\left[\mathcal{H}_{\text{ref}}^{\theta_*} \ \mathcal{H}_{\text{test}}^{\theta}\right]$ that is truncated at order n, it can be easily shown that

$$\mathcal{H}_{\text{test}}^{\theta}\mathcal{Z}_{\text{test}}^{\dagger}\mathcal{Z}_{\text{ref}} - \mathcal{H}_{\text{ref}}^{\theta_*} \neq 0 \quad \text{if} \quad \theta \neq \theta_*. \tag{20}$$

Based on both properties (19) and (20), the damage detection residual is defined on the respective estimates from measurement data as

$$\zeta = \sqrt{N}\,\text{vec}(\hat{\mathcal{H}}_{\text{test}}^{\theta}\hat{\mathcal{Z}}_{\text{test}}^{\dagger}\hat{\mathcal{Z}}_{\text{ref}} - \hat{\mathcal{H}}_{\text{ref}}^{\theta_*}), \tag{21}$$

where $\hat{\mathcal{Z}}_{\text{ref}}$ and $\hat{\mathcal{Z}}_{\text{test}}$ are defined analogously to (17) from the truncated SVD at order n of the juxtaposed Hankel matrix estimates

$$\left[\hat{\mathcal{H}}_{\text{ref}}^{\theta_*} \ \hat{\mathcal{H}}_{\text{test}}^{\theta}\right] = \left[\hat{U}_{\text{s}} \ \hat{U}_{\text{ker}}\right] \begin{bmatrix} \hat{D}_{\text{s}} & 0 \\ 0 & \hat{D}_{\text{ker}} \end{bmatrix} \begin{bmatrix} \hat{V}_{\text{s,ref}}^T & \hat{V}_{\text{s,test}}^T \\ \hat{V}_{\text{ker,ref}}^T & \hat{V}_{\text{ker,test}}^T \end{bmatrix}, \tag{22}$$

as $\hat{\mathcal{Z}}_{\text{ref}} = \hat{D}_{\text{s}}\hat{V}_{\text{s,ref}}^T$, $\hat{\mathcal{Z}}_{\text{test}} = \hat{D}_{\text{s}}\hat{V}_{\text{s,test}}^T$. The use of the normalization factor $\sqrt{N}$ in the residual will become apparent when analyzing the residual distribution in the following.

For a decision if the computed residual belongs to the damaged or to the healthy state, i.e. if there is a significant change in its mean from zero or not, a statistical hyptotheses test is carried out. To achieve such a test, first the statistical distribution of the residual is characterized in the healthy and damaged states, which can be done with the *asymptotic local approach to change detection*[39]. Knowing the distribution properties, the test value is computed, which resembles a weighted Mahalanobis distance.

4.3 | Residual distribution

The statistical distribution of the residual in (21) is unknown, however it can be approximated as Gaussian for a sufficiently large data length N thanks to the asymptotic local approach to change detection[39]. This approach has been used widely for the development of damage detection and localization tests for civil engineering structures[16,34,35,50,51]. In this approach, the close hypotheses

$$\begin{aligned} &\text{H}_0 : \theta = \theta_* \ \text{(healthy state)}, \\ &\text{H}_1 : \theta = \theta_* + \delta/\sqrt{N} \ \text{(damaged state)}, \end{aligned} \tag{23}$$

are formulated, where δ is an unknown but fixed change vector. Subsequently, a statistical test to decide between the null H_0 and the alternative H_1 hypotheses is carried out, with the purpose to detect small deviations from θ_*.

The residual in (21) is a function of the Hankel matrices $\hat{\mathcal{H}}_{\text{ref}}^{\theta_*}$ and $\hat{\mathcal{H}}_{\text{test}}^{\theta}$, therefore it inherits their distribution properties. The output covariance estimates are asymptotically Gaussian, thus it is also the case for the Hankel matrices[52]. The reference Hankel matrix estimate is computed on a data set of length M, and when $M \to \infty$ it satisfies

$$\sqrt{M}\ \text{vec}(\hat{\mathcal{H}}_{\text{ref}}^{\theta_*} - \mathcal{H}_{\text{ref}}^{\theta_*}) \xrightarrow{\mathcal{L}} \mathcal{N}(0, \Sigma_{\text{ref}}), \tag{24}$$

where "$\mathcal{L}$" denotes convergence in distribution, $\mathcal{N}(\mu, \Sigma)$ denotes a Gaussian distributed variable with mean μ and covariance Σ, and Σ_{ref} is the asymptotic reference Hankel matrix covariance. Note that an estimate of Σ_{ref} can be easily obtained from the data, as shown in Appendix A. Similarly, the Hankel matrix estimate computed on the test data of length N is asymptotically Gaussian, and under the hypotheses (23) it holds

$$\text{under H}_0 : \sqrt{N}\ \text{vec}(\hat{\mathcal{H}}_{\text{test}}^{\theta} - \mathcal{H}_{\text{test}}^{\theta_*}) \xrightarrow{\mathcal{L}} \mathcal{N}(0, \Sigma_{\text{test}}), \tag{25}$$

$$\text{under H}_1 : \sqrt{N}\ \text{vec}(\hat{\mathcal{H}}_{\text{test}}^{\theta} - \mathcal{H}_{\text{test}}^{\theta_*}) \xrightarrow{\mathcal{L}} \mathcal{N}(\mathcal{J}_{\theta_*}^{\mathcal{H}_{\text{test}}}\delta, \Sigma_{\text{test}}), \tag{26}$$

where Σ_{test} is the asymptotic covariance of $\hat{\mathcal{H}}_{\text{test}}^{\theta}$, which can be estimated from the data as shown in Appendix A, and $\mathcal{J}_{\theta_*}^{\mathcal{H}_{\text{test}}}$ is the derivative of $\text{vec}(\mathcal{H}_{\text{test}}^{\theta})$ with respect to θ evaluated in θ_*, see also Section 4.3.2.

To propagate the distribution properties (24), (25) and (26) of the Hankel matrices in the reference and tested states to our residual (21), define the joint vectors

$$\hat{h} = \begin{bmatrix} \text{vec}(\hat{\mathcal{H}}_{\text{ref}}^{\theta_*}) \\ \text{vec}(\hat{\mathcal{H}}_{\text{test}}^{\theta}) \end{bmatrix}, \quad h = \begin{bmatrix} \text{vec}(\mathcal{H}_{\text{ref}}^{\theta_*}) \\ \text{vec}(\mathcal{H}_{\text{test}}^{\theta_*}) \end{bmatrix}.$$

To account for different data lengths M and N in the estimates $\hat{\mathcal{H}}_{\text{ref}}^{\theta_*}$ and $\hat{\mathcal{H}}_{\text{test}}^{\theta}$, define the factor $c = \frac{N}{M}$. Then, it follows from (24) that $\text{cov}(\sqrt{N}\text{vec}(\hat{\mathcal{H}}_{\text{ref}}^{\theta_*})) = \text{cov}(\sqrt{\frac{N}{M}}\sqrt{M}\text{vec}(\hat{\mathcal{H}}_{\text{ref}}^{\theta_*})) \approx c\Sigma_{\text{ref}}$. Since both Hankel matrices are computed on different data sets, they are statistically independent, and it follows for the joint distribution[53]

$$\text{under H}_0 : \sqrt{N}\,(\hat{h} - h) \xrightarrow{\mathcal{L}} \mathcal{N}(0, \Sigma_h),$$
$$\text{under H}_1 : \sqrt{N}\,(\hat{h} - h) \xrightarrow{\mathcal{L}} \mathcal{N}(\mathcal{J}_{\theta_*}^h \delta, \Sigma_h),$$

where

$$\mathcal{J}_{\theta_*}^h = \begin{bmatrix} 0 \\ \mathcal{J}_{\theta_*}^{\mathcal{H}_{\text{test}}} \end{bmatrix}, \quad \Sigma_h = \begin{bmatrix} c\Sigma_{\text{ref}} & 0 \\ 0 & \Sigma_{\text{test}} \end{bmatrix}. \tag{27}$$

Since the residual (21) is a function of $\hat{h}$, the delta method[54] can be applied, which allows to characterize the distribution of a function of an asymptotically Gaussian variable as also asymptotically Gaussian, requiring the derivative of the function. In our case, the derivative is given by

$$\mathcal{J}_h^\zeta = \frac{\partial \text{vec}(\mathcal{H}_{\text{test}}^{\theta_*} \mathcal{Z}_{\text{test}}^\dagger \mathcal{Z}_{\text{ref}} - \mathcal{H}_{\text{ref}}^{\theta_*})}{\partial h}. \tag{28}$$

Then it follows with the delta method and property (19) that the residual is asymptotically Gaussian, with the properties

$$\text{under H}_0 : \zeta \xrightarrow{\mathcal{L}} \mathcal{N}(0, \Sigma_\zeta), \tag{29}$$
$$\text{under H}_1 : \zeta \xrightarrow{\mathcal{L}} \mathcal{N}(\mathcal{J}_{\theta_*}^\zeta \delta, \Sigma_\zeta), \tag{30}$$

where $\mathcal{J}_{\theta_*}^\zeta = \mathcal{J}_h^\zeta \mathcal{J}_{\theta_*}^h$ is the residual sensitivity with respect to the chosen parametrization, and $\Sigma_\zeta = \mathcal{J}_h^\zeta \Sigma_h \mathcal{J}_h^{\zeta T}$ is the residual covariance. Both are detailed in the following.

4.3.1 | Residual covariance

The difficulty in the evaluation of the residual covariance lies in the computation of the derivative $\mathcal{J}_h^\zeta$, which requires in particular the derivatives of the matrices $\mathcal{Z}_{\text{ref}}$ and $\mathcal{Z}_{\text{test}}$ and thus derivatives of the SVD[55]. After a lengthy and technical derivation, the expression for the residual covariance $\Sigma_\zeta = \mathcal{J}_h^\zeta \Sigma_h \mathcal{J}_h^{\zeta T}$ boils down to

$$\Sigma_\zeta = \mathcal{J}_{\mathcal{H}_{\text{ref}}}^\zeta c\Sigma_{\text{ref}} (\mathcal{J}_{\mathcal{H}_{\text{ref}}}^\zeta)^T + \mathcal{J}_{\mathcal{H}_{\text{test}}}^\zeta \Sigma_{\text{test}} (\mathcal{J}_{\mathcal{H}_{\text{test}}}^\zeta)^T, \tag{31}$$

where $\mathcal{J}_{\mathcal{H}_{\text{ref}}}^\zeta = I_{(p+1)r} \otimes U_{\text{ker}} U_{\text{ker}}^T$ and $\mathcal{J}_{\mathcal{H}_{\text{test}}}^\zeta = (\mathcal{Z}_{\text{test}}^\dagger \mathcal{Z}_{\text{ref}})^T \otimes U_{\text{ker}} U_{\text{ker}}^T$. Note that both covariances Σ_{ref} and Σ_{test} referring to the reference and to the test data contribute to the residual covariance in (31), since the residual depends on both the reference and the test data. The covariance from the reference state is weighted with factor $c = \frac{N}{M}$. In practice, when more data is collected in the reference state than in the tested state, i.e. $M > N$, c is smaller than one and the covariance contribution related to the reference data is small compared to the test data. In this case, the covariance related to the test data is the predominant source of uncertainty. The opposite applies when few data is available in the reference state, i.e. $M < N$, then c is large and the contribution of the covariance related to the reference state becomes predominant.

An estimate $\hat{\Sigma}_\zeta$ of the residual covariance in (31) can be computed with covariance estimates $\hat{\Sigma}_{\text{ref}}$ and $\hat{\Sigma}_{\text{test}}$ of the Hankel matrices (see Appendix A) and the matrices $\hat{\mathcal{Z}}_{\text{ref}}$ and $\hat{\mathcal{Z}}_{\text{test}}$ from the SVD of the juxtaposed Hankel matrix estimates in (22). Since $\hat{\Sigma}_\zeta$ is an estimate of the asymptotic covariance and U_{ker} is independent of the excitation, $\hat{U}_{\text{ker}}$ can be obtained once in the reference state and does not need to be recomputed on the test data.

4.3.2 | Residual sensitivity with respect to system parameter

Similarly as in the previous section, the derivative $\mathcal{J}_h^\zeta$ is required to evaluate the residual sensitivity $\mathcal{J}_{\theta_*}^\zeta = \mathcal{J}_h^\zeta \mathcal{J}_{\theta_*}^h$. Note that the sensitivity is evaluated in the healthy state under parameter θ_*. Combining properties (19), (27) and (28), the residual sensitivity boils down to

$$\mathcal{J}_{\theta_*}^\zeta = \left((\mathcal{Z}_{\text{ref}}^\dagger \mathcal{Z}_{\text{ref}})^T \otimes U_{\text{ker}} U_{\text{ker}}^T \right) \frac{\partial \text{vec}(\mathcal{H}_{\text{ref}}^\theta)}{\partial \theta}(\theta_*). \tag{32}$$

Thanks to the factorization of the Hankel matrix $\mathcal{H}^{\theta}_{\text{ref}} = \mathcal{O}^{\theta}_{\text{ref}} C^{\theta}_{\text{ref}}$ into observability and controllability matrices in (3), it follows with the product rule

$$\frac{\partial \text{vec}(\mathcal{H}^{\theta}_{\text{ref}})}{\partial \theta} = \left(C^{\theta_* T}_{\text{ref}} \otimes I_{(p+1)r} \right) \frac{\partial \text{vec}(\mathcal{O}^{\theta}_{\text{ref}})}{\partial \theta} + \left(I_{qr} \otimes \mathcal{O}^{\theta_*}_{\text{ref}} \right) \frac{\partial \text{vec}(C^{\theta}_{\text{ref}})}{\partial \theta}.$$

Plugging this into (32), and using the properties $U^T_{\text{ker}} \mathcal{O}^{\theta_*}_{\text{ref}} = 0$ and $\mathcal{H}^{\theta_*}_{\text{ref}} = U_s \mathcal{Z}_{\text{ref}} = \mathcal{O}^{\theta_*}_{\text{ref}} C^{\theta_*}_{\text{ref}}$ leads to

$$\mathcal{J}^{\zeta}_{\theta_*} = \left(C^{\theta_* T}_{\text{ref}} \otimes U_{\text{ker}} U^T_{\text{ker}} \right) \mathcal{J}^{\mathcal{O}}_{\theta_*}, \quad \text{where} \quad \mathcal{J}^{\mathcal{O}}_{\theta_*} = \frac{\partial \text{vec}(\mathcal{O}^{\theta}_{\text{ref}})}{\partial \theta}(\theta_*). \tag{33}$$

Since the observability matrix depends on the system matrices A and C and thus on the modal parameters, its derivative with respect to the modal parameters can be analytically computed[50]. Finally, the derivative $\mathcal{J}^{\zeta}_{\theta_*}$ with respect to the chosen system parametrization depends on its link to the modal parameters. Here, the chain system will be parametrized with its analytical stiffnesses, which are connected to the modal parameters. In this case, the derivative of the observability matrix with respect to the system parameters writes

$$\mathcal{J}^{\mathcal{O}}_{\theta_*} = \mathcal{J}^{\mathcal{O}}_{\text{mod}} \mathcal{J}^{\text{mod}}_{\theta_*},$$

where $\mathcal{J}^{\mathcal{O}}_{\text{mod}}$ is the derivative of the observability matrix with respect to the modal parameters, and $\mathcal{J}^{\text{mod}}_{\theta_*}$ is the derivative of the modal parameters with respect to the selected structural system parameters. The computation of these derivatives is detailed e.g. in[50,51].

The residual derivative $\mathcal{J}^{\zeta}_{\theta_*}$ as developed in (33) only depends on matrices that can be computed in the reference state, and no quantities related to the tested state are involved. Hence, possible changes in the excitation properties in the tested state do not impact the residual derivative, which is thus invariant towards a change in the excitation properties. Consequently, the residual mean $\mathcal{J}^{\zeta}_{\theta_*} \delta$ (see (30)) is indeed unaffected by changes in the excitation properties, which is a key result of this paper.

An estimate $\hat{\mathcal{J}}^{\zeta}_{\theta_*}$ of the residual sensitivity in (33) can be computed using estimates of U_{ker}, $C^{\theta_*}_{\text{ref}}$ and $\mathcal{J}^{\mathcal{O}}_{\text{mod}}$ in the reference state of the structure. If the chosen parametrization goes beyond the modal parameters and involves structural parameters, the derivative $\mathcal{J}^{\text{mod}}_{\theta_*}$ is usually obtained in connection with an analytical model[50].

4.4 | Damage detection test

Based on the local approach, the considered residual in (29) is asymptotically Gaussian distributed under both hypotheses. Hence a decision between the latter to decide if the system is healthy or damaged can be achieved by applying the Generalized Likelihood ratio (GLR) test[16,34,39]. In this section, the test is developed for the cases of known and unknown system parametrization, and showcased on the mass spring chain example from Section 3.1.

4.4.1 | Parametric test

Testing $\delta = 0$ (no damage) against $\delta \neq 0$ (indicating damage) based on the residual distribution (29)–(30) yields the test statistic[16]

$$t = \zeta^T \hat{\Sigma}^{-1}_{\zeta} \hat{\mathcal{J}}^{\zeta}_{\theta_*} \left(\hat{\mathcal{J}}^{\zeta T}_{\theta_*} \hat{\Sigma}^{-1}_{\zeta} \hat{\mathcal{J}}^{\zeta}_{\theta_*} \right)^{-1} \hat{\mathcal{J}}^{\zeta T}_{\theta_*} \hat{\Sigma}^{-1}_{\zeta} \zeta \,, \tag{34}$$

which is asymptotically χ^2 distributed with $d = \text{rank}(\mathcal{J}^{\zeta}_{\theta_*})$ degrees of freedom and non-centrality parameter

$$\lambda = \delta^T \mathcal{J}^{\zeta T}_{\theta_*} \Sigma^{-1}_{\zeta} \mathcal{J}^{\zeta}_{\theta_*} \delta \tag{35}$$

in the damaged state. Thus, the test value resulting from (34) should be compared to a threshold that is set up in the reference state[35]. A numerically efficient computation of the test value is developed in Appendix B. Note that the test t resembles a weighted Mahalanobis distance: the residual ζ describes the Hankel matrix difference between the reference and tested states of the structure that is normalized with respect to excitation. Weighting this difference by its covariance and sensitivity as $\tilde{\zeta} = \hat{\mathcal{J}}^{\zeta T}_{\theta_*} \hat{\Sigma}^{-1}_{\zeta} \zeta$, the test t describes its Mahalanobis distance $t = \tilde{\zeta}^T \hat{\Sigma}^{-1}_{\tilde{\zeta}} \tilde{\zeta}$, where $\hat{\Sigma}_{\tilde{\zeta}} = \text{cov}(\tilde{\zeta}) = \hat{\mathcal{J}}^{\zeta T}_{\theta_*} \hat{\Sigma}^{-1}_{\zeta} \hat{\mathcal{J}}^{\zeta}_{\theta_*}$.

The distribution of the test in the healthy state depends only on the rank of the residual derivative, which has been shown to be independent of the excitation properties in Section 4.3.2. This means that the test computed in the healthy state of the structure is robust towards changes in the excitation properties, which is a key property of the developed test. Hence, excitation changes do not lead to false alarms. In the damaged state, the distribution of the test shifts with the non-centrality parameter $\lambda > 0$ in (35), which depends on the residual covariance Σ_{ζ}. Since this covariance depends in part on the test data, the distribution of the test in the damaged state may change (slightly) with changing excitation properties.

In the following, the performance of the parametric test is demonstrated on simulations of the chain-like system introduced in Section 3.1. Figure 6 (left) displays the evolution of the test over time for three different states of the system, namely one healthy and two damage states. As it can be seen, the test is able to separate the healthy state from the different damages despite being computed for different properties of the excitation. Figure 6 (right) displays the same type of information for Q changing all the time for each data set, showing that the damage can be detected without any prior knowledge of the excitation properties. As expected, no false alarms are present in the healthy state.

To illustrate the distribution of the test statistics, Monte Carlo simulations are conducted for the considered excitation cases. In Figure 7 (left) the distributions of the test for Monte Carlo simulations are shown for three different excitation covariance matrices Q. In the healthy case, all three distributions are superposed, showing the robustness of the test to the excitation changes and exhibiting no false alarms. The test values due to damage are well separated from the ones corresponding to the healthy state. They show some fluctuations due to Q in the damage states, which does not impair the detection. In Figure 7 (right), the excitation covariance is changed randomly between each simulated data set. It shows a good separation between the test value computed on the healthy structure and the damaged states, without any knowledge of the constantly changing excitation properties. Note that the mean of the test in the healthy state is stable and very close to the theoretical value, which is the rank of the derivative $\mathcal{J}^{\zeta}_{\theta_*}$. Consequently, a threshold for detection corresponding to the quantiles of the theoretical distribution of the reference test values can be determined a priori for assessing that damage occurred in the structure.

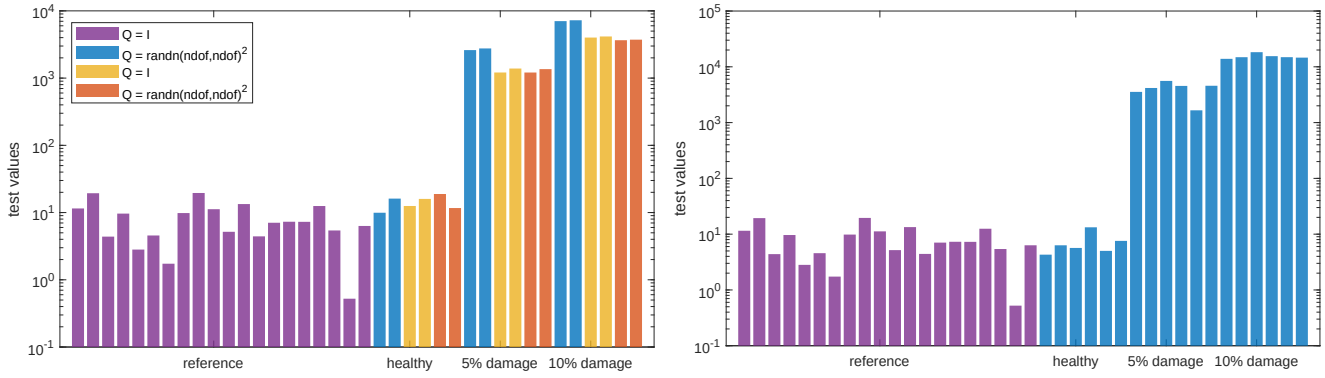

FIGURE 6 Damage detection with parametric test based on robust normalization. Three different excitation covariances in the tested data sets (left), random excitation covariance changing for each tested data set (right).

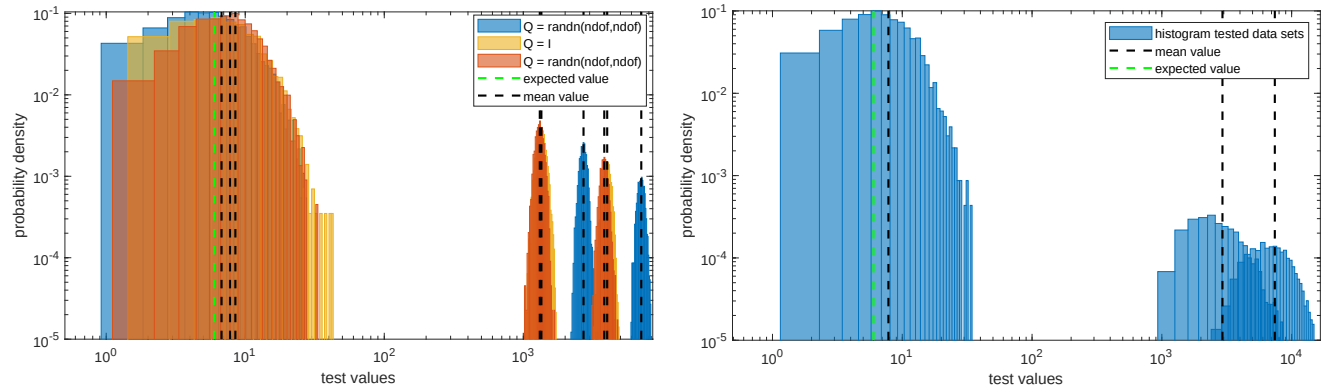

FIGURE 7 Histograms of parametric damage detection test. Three different excitation covariances in the tested data sets (left), random excitation covariance changing for each tested data set (right).

4.4.2 | Non-parametric test

When no parametrization is considered, a simple test can be carried out directly on the residual, assuming any change in the mean of the residual in the damaged state in (30). This corresponds to $\mathcal{J}_{\theta_*}^{\zeta} = I$, and the test boils down to its non-parametric version

$$t_{\text{np}} = \zeta^T \hat{\Sigma}_{\zeta}^{-1} \zeta. \tag{36}$$

This test is asymptotically χ^2 distributed, with non-centrality parameter $\lambda > 0$ in the damaged state. For a decision about damage, the test value should thus be compared to a threshold that can obtained empirically from the realizations of the test in the reference state. Note that the test t_{np} also resembles a Mahalanobis distance, similar to the parametric test.

The non-parametric test inherits the robustness towards changes in the excitation covariance from the parametric test, where it has been shown that the residual mean and thus the test in the healthy state of the structure are unaffected by those changes. Hence, excitation changes do not lead to false alarms in the non-parametric test.

In the following the results from the non-parametric test are presented on simulations of the chain-like system. The protocol is the same as in the previous section. The results in Figure 8 (left) are quite similar, where values of the damage detection test for all three different Q are well separated and the damage is well detected. As expected, no false alarm is present in the reference state. Test values for completely unknown and changing Q are plotted in Figure 8 (right), showing no false alarms and a good detection of the damages in both damage states. This is also confirmed in Monte Carlo simulations for three distinct excitation cases in Figure 9 (left), as well as for arbitrary random excitation cases in Figure 9 (right), where the test in the damaged states is well separated from the healthy state, and no false alarms are present. Notice that the mean value of the test in the healthy state is quite high and unpredictable, in contrast to the parametric test. This is due to the lack of the Jacobian in the computation of the

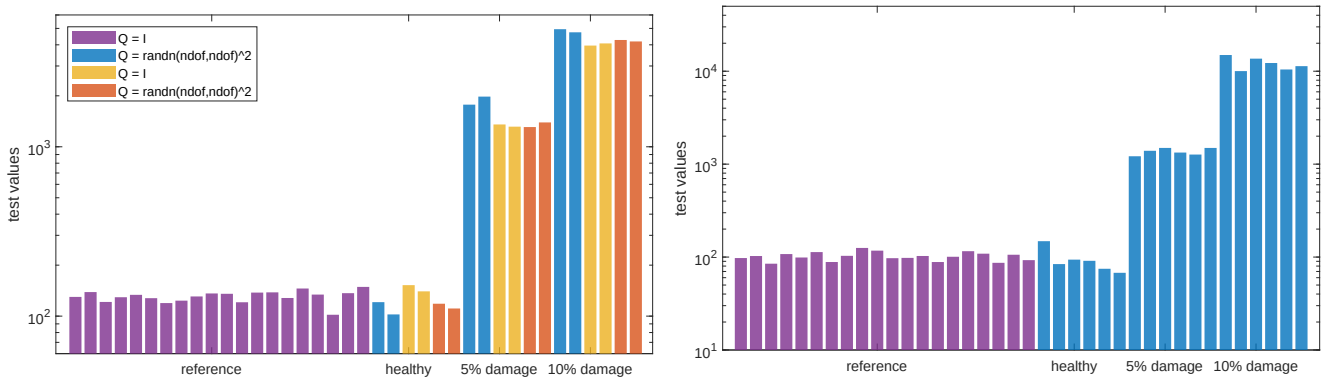

FIGURE 8 Damage detection with non-parametric test. Three different excitation covariances in the tested data sets (left), random excitation covariance changing for each tested data set (right).

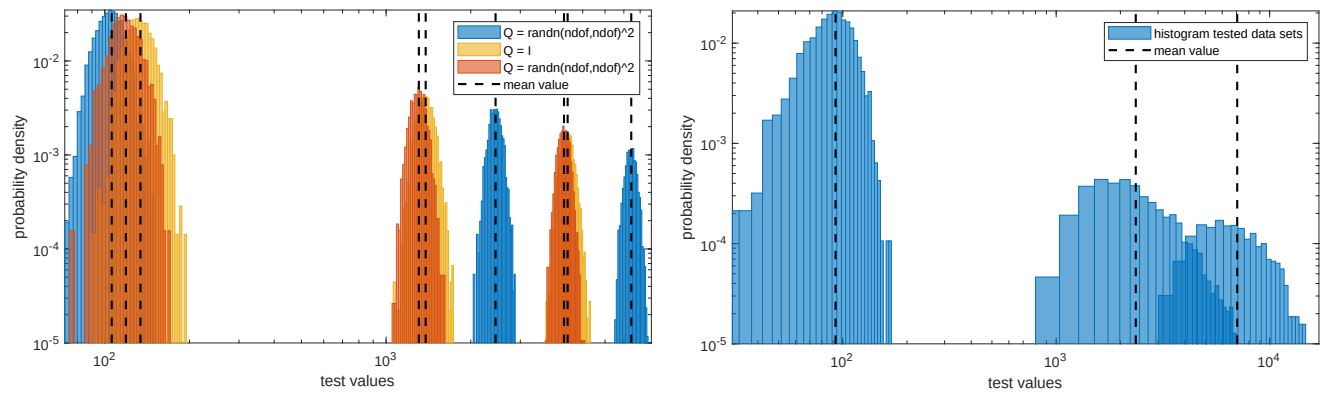

FIGURE 9 Distribution of non-parametric test based on robust normalization. Three different excitation covariances in the tested data sets (left), random excitation covariance changing for each tested data set (right).

test, which would take into account the sensitivity of the test with respect to each of the parameters. Therefore, when using such a Jacobian the mean value of the test can be predicted, and a threshold for damage can be theoretically established. However, it is still possible to determine a threshold empirically with the non-parametric test based on realizations from the healthy state.

4.5 | Algorithmic summary of the developed methods

The algorithmic procedure devised for the proposed damage detection tests is summarized below. Since for $\mathcal{J}_{\theta_*}^{\zeta} = I$ the parametric test boils down to its rudimentary non-parametric equivalent, the procedure below outlines the computational scheme only for the parametric test. First the outline for processing the measurements in the reference state of the structure is given in Algorithm 1. Subsequently, when the characteristics of the reference are computed, the procedure for the computation of the parametric damage detection test for any data set is given in Algorithm 2. A brief schematic of the damage detection procedure is illustrated on a flowchart in Figure 10.

Algorithm 1: Parametric test (34): processing the reference state

Input : reference data set $\{y_k\}_{k=1,\dots,M}$;
parameters: output covariance lags p and q, model order n, number of data blocks n_b, parametrization θ_*, confidence level γ

Output: reference characteristics: $\hat{\mathcal{H}}_{\text{ref}}$, $\hat{\mathcal{B}}$, $\hat{\mathcal{J}}_s$, $\hat{\Sigma}_{\text{ref}}^{1/2}$ and threshold l

1 compute $\hat{\mathcal{H}}_{\text{ref}}$ from $\{y_k\}_{k=1,\dots,M}$ in (5) ;
2 compute the left kernel $\hat{U}_{\text{ker}}$ from $\hat{\mathcal{H}}_{\text{ref}}$ using SVD, and $\hat{\mathcal{B}} = I_{(p+1)r} \otimes \hat{U}_{\text{ker}}$;
3 compute the Jacobian matrix $\hat{\mathcal{J}}_s$ after (B3) and (33) ;
4 compute $\hat{\Sigma}_{\text{ref}}^{1/2}$ from $\{y_k\}_{k=1,\dots,M}$ in (A1) ;
5 compute l as γ-quantile of χ^2 distribution with $d = \text{rank}(\hat{\mathcal{J}}_s)$ degrees of freedom

Algorithm 2: Parametric test (34): statistical testing of a data set

Input : reference characteristics: $\hat{\mathcal{H}}_{\text{ref}}$, $\hat{\mathcal{B}}$, $\hat{\mathcal{J}}_s$, $\hat{\Sigma}_{\text{ref}}^{1/2}$, reference data length M ;
parameters: output covariance lags p and q, model order n, number of data blocks n_b ;
test data set $\{y_k\}_{k=1,\dots,N}$

Output: test value t

1 compute $\hat{\mathcal{H}}_{\text{test}}$ from $\{y_k\}_{k=1,\dots,N}$ in (5) ;
2 compute $\hat{\mathcal{Z}}_{\text{ref}} = \hat{D}_s \hat{V}_{s,\text{ref}}^T$ and $\hat{\mathcal{Z}}_{\text{test}} = \hat{D}_s \hat{V}_{s,\text{test}}^T$ from joint SVD of $[\hat{\mathcal{H}}_{\text{ref}} \;\; \hat{\mathcal{H}}_{\text{test}}]$ in (22) ;
3 compute residual $\zeta = \sqrt{N}\,\text{vec}(\hat{\mathcal{H}}_{\text{test}} \hat{\mathcal{Z}}_{\text{test}}^{\dagger} \hat{\mathcal{Z}}_{\text{ref}} - \hat{\mathcal{H}}_{\text{ref}})$ in (21) ;
4 compute $\hat{\Sigma}_{\text{test}}^{1/2}$ from $\{y_k\}_{k=1,\dots,N}$ in (A1) and $c = \frac{N}{M}$;
5 compute $\hat{\mathcal{L}} = \left[\hat{\mathcal{B}}^T \sqrt{c}\hat{\Sigma}_{\text{ref}}^{1/2} \quad \left(\hat{\mathcal{Z}}_{\text{ref}}^{\dagger} \hat{\mathcal{Z}}_{\text{ref}}\right)^T \otimes I_{(p+1)r-n}\right) \hat{\mathcal{B}}^T \hat{\Sigma}_{\text{test}}^{1/2}\right]$ and QR decomposition of $\hat{\mathcal{L}}^{\dagger} \hat{\mathcal{J}}_s P = \hat{\mathcal{Q}} \hat{\mathcal{R}}$ in (B4) ;
6 compute $a = \tilde{\mathcal{Q}}^T \hat{\mathcal{L}}^{\dagger} \hat{\mathcal{B}}^T \zeta$ where $\tilde{\mathcal{Q}}$ are the columns of $\hat{\mathcal{Q}}$ that correspond to non-zero diagonal entries in $\hat{\mathcal{R}}$;
7 compute the test value $t = a^T a$ in (B5)

5 | APPLICATION: SIMULATION OF A MONO BUCKET FOUNDATION

This section is devoted to the application of the proposed damage detection test on data simulated based on a large finite element (FE) model of a novel offshore foundation concept, namely a Mono Bucket foundation[56,57]. The sole purpose of using the FE model is to simulate the response of the foundation towards ambient excitation for two realistic damage scenarios. Previously, a high sensitivity to detect different damages in the shaft of the foundation was observed[58]. The following application examines the same damage scenarios, however focuses on the impact of changing excitation conditions on the developed damage detection metrics.

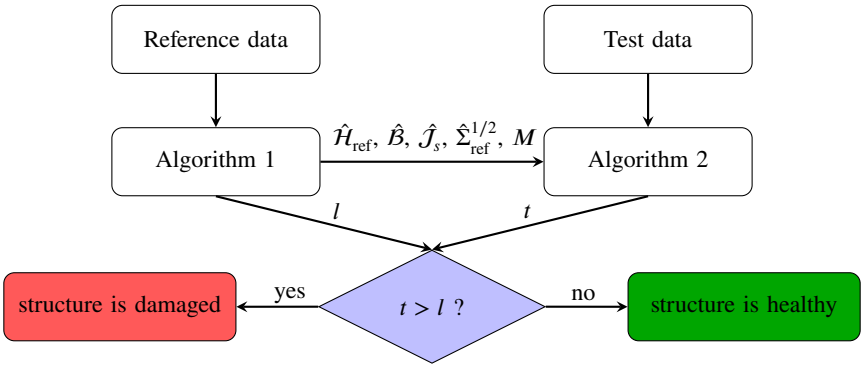

FIGURE 10 Damage detection flowchart

The FE model of the foundation contains 8589 first-order shell elements, 8414 nodes and, consequently, 50484 degrees of freedom (DOF), and is modeled after the substructure of an offshore structure investigated in[59,60]. For the sake of simulation, proportional damping is assumed, where the damping matrix is defined such that each mode has a damping ratio of 1%. The translational and rotational DOF are constrained to zero at the bottom elements of the model. The excitation is modeled as a white noise signal of positive definite covariance matrix Q whose entries are computed as $Q = a \cdot bb^T$, where a is a random positive scalar between 1 and 10 and b is a matrix drawn from a standard normal distribution. The resultant input signal is applied on the top 42 DOF of the model. The structural acceleration data used for damage detection are simulated with a sampling frequency of 50 Hz at 10 DOF, representing measurements at five biaxial sensors placed along the shaft of the foundation. This allows to observe four pairs of a closely spaced bending modes of the foundation. The model and its real-life representation are depicted in Figure 11.

Two damage scenarios are considered that consist of the reduction of thickness of elements in the connections A and B (see Figure 11). Firstly the thickness of 8 elements is reduced by 15%, which corresponds to the designed corrosion allowance of external surfaces of the foundations for offshore wind turbines located at the North Sea[61]. Secondly, the reduction in thickness of the same elements progresses to 40%. Those changes are then reflected in the measurement data, on which the damage detection residual is computed. Inflicted damages influence the exact natural frequencies of the FE model, which are presented in Table

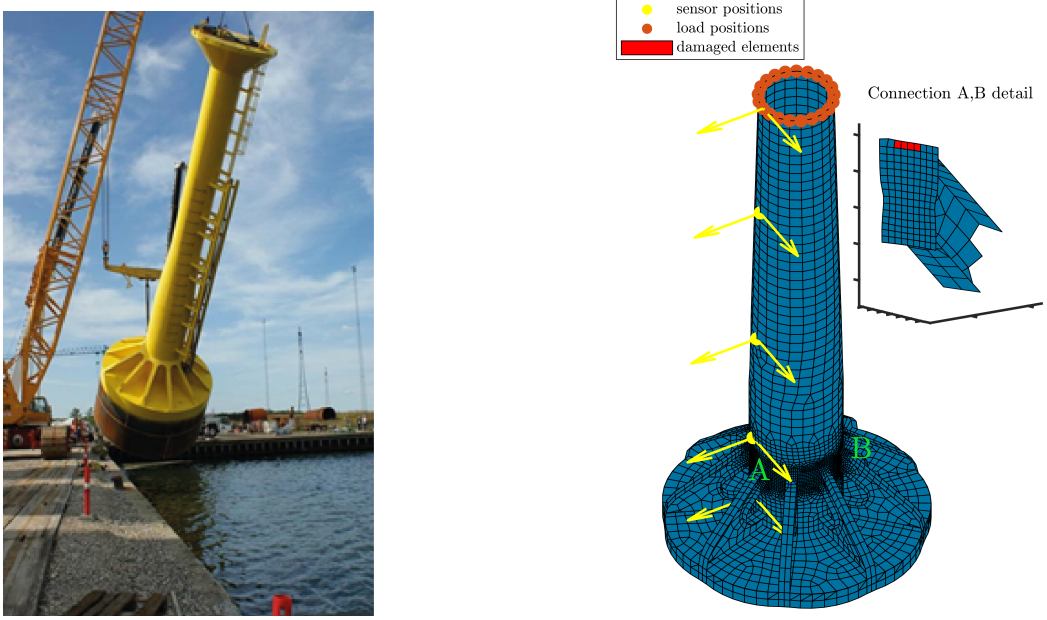

FIGURE 11 Mono Bucket foundation for offshore meteorological mast at Horns Rev 2 (left). FE model of the foundation (right).

TABLE 2 Exact natural frequencies f_i (Hz) of the Mono Bucket foundation model.

Structural state	f_1	f_2	f_3	f_4	f_5	f_6	f_7	f_8
Healthy	5.6913	5.6953	6.4076	6.4095	14.0879	14.1024	19.2749	19.2777
Damage case 1	5.6895	5.6940	6.4075	6.4093	14.0875	14.1006	19.2747	19.2776
Damage case 2	5.6868	5.6920	6.4073	6.4089	14.0867	14.0978	19.2744	19.2773

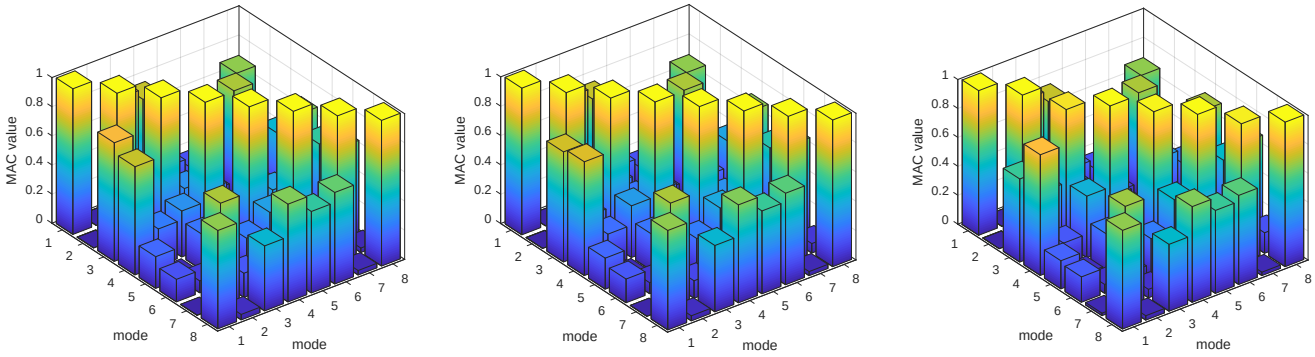

FIGURE 12 MAC values computed between exact mode shapes at discrete sensor positions corresponding to the healthy model (left), the healthy model and the first damage scenario (middle), and the healthy model and the second damage scenario (right).

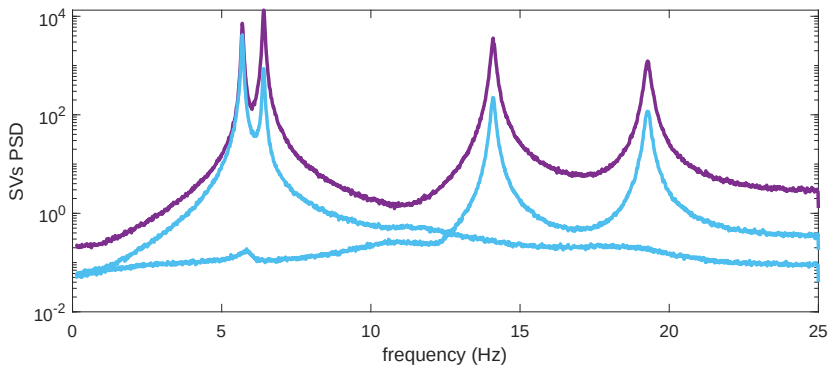

FIGURE 13 Singular values of PSD's estimated from the simulated healthy data set.

2. It can be viewed that the reduction in the natural frequencies is small and reaches up to 0.08% for the first mode of the second damage case. The applied damages also perturb the mode shape vectors. The change in mode shapes can be observed when comparing the corresponding MAC values computed between the mode shapes of the healthy and damaged models, which are illustrated in Figure 12. The maximum change in the auto-MAC occurs for the 7-th mode shape vector and yields 0.65%, and more significant changes occur in the cross-MACs.

Firstly, the damage campaign is simulated with 20 data sets of length $N = 200{,}000$ in the healthy and both damage states. The data set in the reference state is simulated with length $M = 1{,}000{,}000$. To illustrate the spectral content of the simulated signals, the three first singular values of the Power Spectral Density (PSD) matrix estimated from the first healthy data set are shown in Figure 13. It can be viewed that the 4 pairs of modes are well excited by the applied input signal.

To evaluate the performance of the developed damage detection test, the obtained results are compared to the empirical d_4 metric introduced in Section 3.2. The analysis is made with model order $n = 16$ and $p + 1 = 3$ time lags to compute the Hankel matrices. The number of blocks for the covariances of the reference and the tested Hankel matrices is selected at $n_b = 800$. The results of the test values from the d_4 metric (13) and the developed non-parametric test (36) are depicted in Figure 14. It can

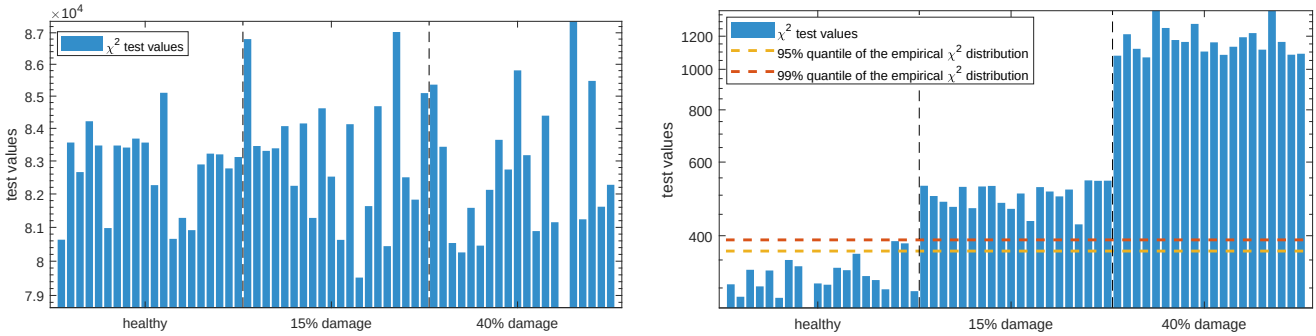

FIGURE 14 Damage detection d_4 (left). Damage detection with non-parametric test (right).

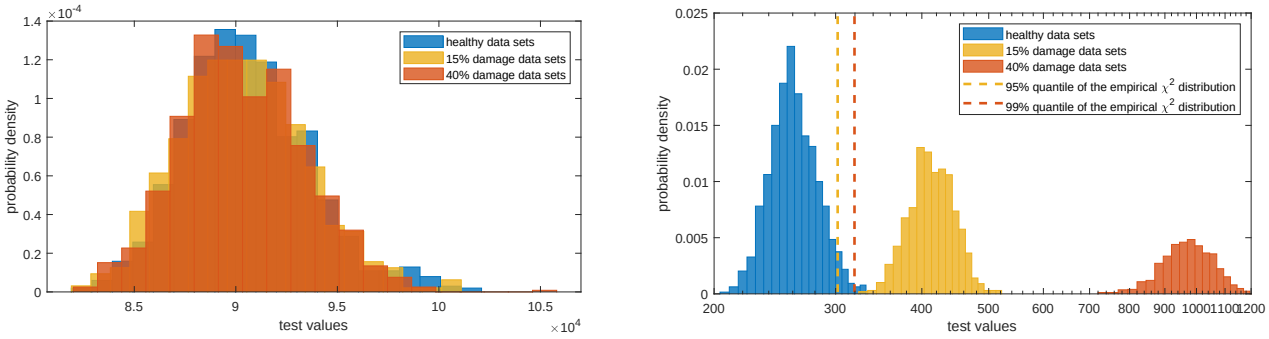

FIGURE 15 Monte Carlo histogram for the d_4 approach (left) and the non-parametric testing (right).

be viewed that while the empirical d_4 metric cannot detect any damages inflicted to the model, the non-parametric test with the robust residual successfully detects both damage scenarios.

To illustrate the distribution of the test statistics, Monte Carlo experiment with 1000 simulations of each damage case is conducted, and its results are illustrated in Figure 15. As expected, inflicted damages are clearly detected with the non-parametric test, despite possible fluctuations in the unknown ambient excitation. Moreover, a clear separation between safe and damaged states is observed, which is contrary to the results obtained with d_4 metric where the histograms of test values corresponding to different damage scenarios are indistinguishable.

While the damages are clearly detected with the non-parametric test, the definition of a threshold requires multiple evaluation of the non-parametric test in the healthy state. The parametric test (34) that is shown next, is free of this shortcoming. The system is parametrized with the first 8 modal parameters of the FE model, and the derivative of the observability matrix $\mathcal{J}^{\mathcal{O}}_{\text{mod}}$ w.r.t. the modal parameters is computed[50,51]. The rank of this derivative is $\text{rank}(\mathcal{J}^{\mathcal{O}}_{\text{mod}}) = 16$, which equals to the degrees of freedom of χ^2 distribution of the parametric test values in the healthy state, and allows to establish damage detection thresholds prior to the analysis. The parametric test behaves similarly to the non-parametric test, with the added benefit of its mean being more predictable. Indeed, the mean value of the parametric test from Monte Carlo experiment is very close to its expected theoretical value, as illustrated in Figure 16. The 95% and 99% quantiles of the underlying χ^2 distribution of the test values in the healthy state correspond to 5% and 1% false alarm rate respectively, and are precise enough to be used a priori as damage detection thresholds. Notice that using more samples would yield more accurate estimated test values, closer to their theoretical expected values.

Both non-parametric and parametric tests show behavior that is superior to the other state of art Mahalanobis distance-based methods presented before. All the test values corresponding to the data sets in the damaged states are above the thresholds, indicating 0% false negative tests for these damages. Furthermore, the proposed approaches are able to discriminate different levels of the damage as shown by the clear separation of the histograms in Figure 15 (right) and Figure 16 (right). Despite the parametric approach being the recommended option, notice that the non-parametric test is quite practicable due to its simplicity,

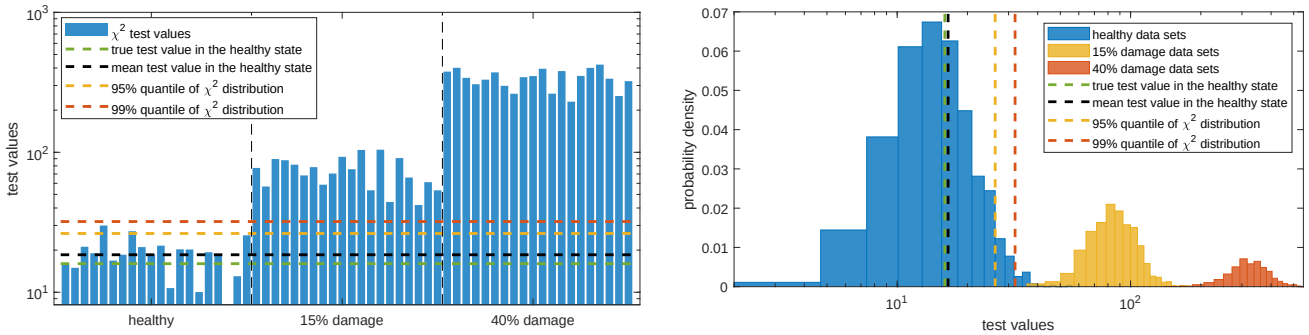

FIGURE 16 Damage detection with parametric approach (left). Monte Carlo histogram of damage indicators for the parametric testing (right).

provided that empirical thresholds are defined for example by monitoring the structure over some period of time in the healthy state.

6 | CONCLUSION

In this paper, a new Gaussian residual for damage detection has been derived based on the Mahalanobis distance between Hankel matrices in different states of the structure, which is normalized with respect to changes in the unknown ambient excitation covariance. In the statistical analysis of the residual the Mahalanobis distance has been related to the local approach framework for Gaussian residuals, and the associated damage detection test has been developed. The proposed method has been shown to be robust towards false alarms in the healthy state of the structure under changes in the excitation properties, a feature that is critical for its practical application in structural monitoring systems. Furthermore, the developed method takes into account the uncertainty inherent to both the reference and the tested data sets, unlike in previous approaches, which yields an improved noise robustness. The new method has been applied to a simulation of an offshore foundation based on a large FE model. It has been demonstrated that it exhibits no outliers in the healthy state, thus avoiding false alarms, and that it is able to detect damage that is based on changes in few elements of the FE model with both the non-parametric and the parametric test variants. While thresholds for detection can be set empirically with the non-parametric test, they can be defined a priori with the parametric test when taking into account the residual sensitivities, improving the capabilities of the test. Future work includes the validation of the developed approach on experimental data of a real large scale structure tested under changing excitation conditions, as well as its extension to damage localization based on the parametric version of the test.

ACKNOWLEDGMENTS

Søren Andreas Nielsen, Jeppe Pryds Hansen and Laura Garcia Castillo from Universal Foundation A/S are acknowledged for the insight on the Mono Bucket foundation model.

□

APPENDIX

A ESTIMATING THE COVARIANCE OF THE HANKEL MATRIX

The residual covariance (31) depends on the covariance of vectorized Hankel matrices $\mathrm{vec}(\hat{\mathcal{H}}_{\mathrm{ref}}^{\theta_*})$ and $\mathrm{vec}(\hat{\mathcal{H}}_{\mathrm{test}}^{\theta})$. Their consistent estimates can be computed from the covariance of the sample mean [35] as recalled in the following.

Let $\hat{\mathcal{H}}$ be a Hankel matrix estimate computed from a data set $\{y_k\}_{k=1\dots N}$ of length N. The estimate $\hat{\mathcal{H}}$ can be written as a mean of $j = 1 \dots n_b$ Hankel matrices computed over n_b blocks of available data, each of length N_b such that $\hat{\mathcal{H}} = (1/n_b)\sum_{j=1}^{n_b} \hat{\mathcal{H}}^{(j)}$ where $n_b \cdot N_b = N$. Then a consistent estimate of the covariance of the vectorized Hankel matrix $\Sigma_{\mathcal{H}}$ writes

$$\hat{\Sigma}_{\mathcal{H}} = \frac{N_b}{n_b - 1} \sum_{j=1}^{n_b} \operatorname{vec}(\hat{\mathcal{H}}^{(j)} - \hat{\mathcal{H}}) \operatorname{vec}(\hat{\mathcal{H}}^{(j)} - \hat{\mathcal{H}})^T,$$

and a factorization $\hat{\Sigma}_{\mathcal{H}} = \hat{\Sigma}_{\mathcal{H}}^{1/2}(\hat{\Sigma}_{\mathcal{H}}^{1/2})^T$ for an efficient computation is given directly by

$$\hat{\Sigma}_{\mathcal{H}}^{1/2} = \begin{bmatrix} h_1 & h_2 & \dots & h_{n_b} \end{bmatrix}, \quad \text{where} \quad h_j = \sqrt{\frac{N_b}{n_b - 1}} \operatorname{vec}(\hat{\mathcal{H}}^{(j)} - \hat{\mathcal{H}}). \tag{A1}$$

B NUMERICALLY EFFICIENT COMPUTATION OF PARAMETRIC TEST

The direct computation of the parametric test (34) may be numerically unstable when the estimate of the covariance matrix Σ_ζ is rank deficient or badly conditioned[16,35]. For the derivation of a numerically stable test, first the computation of Σ_ζ in (31) is reformulated to exploit its factorization. Define

$$\mathcal{B} = I_{(p+1)r} \otimes U_{\text{ker}}, \quad \mathcal{L} = \begin{bmatrix} \mathcal{B}^T (c\Sigma_{\text{ref}})^{1/2} & \left((\mathcal{Z}_{\text{test}}^\dagger \mathcal{Z}_{\text{ref}})^T \otimes I_{(p+1)r-n} \right) \mathcal{B}^T \Sigma_{\text{test}}^{1/2} \end{bmatrix},$$

then it follows $\Sigma_\zeta = \mathcal{B}\mathcal{L}(\mathcal{B}\mathcal{L})^T$ and its (pseudo-)inverse can be written as

$$\Sigma_\zeta^\dagger = \mathcal{B}{\mathcal{L}^\dagger}^T \mathcal{L}^\dagger \mathcal{B}^T, \tag{B2}$$

since $\mathcal{B}$ is a matrix with orthogonal columns, $\mathcal{B}^T\mathcal{B} = I$. The matrix square roots $\Sigma_{\text{ref}}^{1/2}$ and $\Sigma_{\text{test}}^{1/2}$ can be directly estimated from (A1). Second, matrix $\mathcal{B}$ is factored from derivative (33) as

$$\mathcal{J}_{\theta_*}^\zeta = \left({C_{\text{ref}}^{\theta_*}}^T \otimes U_{\text{ker}} U_{\text{ker}}^T \right) \mathcal{J}_{\theta_*}^{\mathcal{O}} = \mathcal{B} \left({C_{\text{ref}}^{\theta_*}}^T \otimes U_{\text{ker}}^T \right) \mathcal{J}_{\theta_*}^{\mathcal{O}} = \mathcal{B}\mathcal{J}_s. \tag{B3}$$

Now, plugging (B2) and (B3) into the definition of the test in (34), it follows

$$\begin{aligned} t &= \zeta^T \mathcal{B}{\mathcal{L}^\dagger}^T \mathcal{L}^\dagger \mathcal{B}^T \mathcal{B}\mathcal{J}_s \left((\mathcal{B}\mathcal{J}_s)^T \mathcal{B}{\mathcal{L}^\dagger}^T \mathcal{L}^\dagger \mathcal{B}^T \mathcal{B}\mathcal{J}_s \right)^\dagger (\mathcal{B}\mathcal{J}_s)^T \mathcal{B}{\mathcal{L}^\dagger}^T \mathcal{L}^\dagger \mathcal{B}^T \zeta \\ &= \zeta^T \mathcal{B}{\mathcal{L}^\dagger}^T \mathcal{L}^\dagger \mathcal{J}_s \left(\mathcal{J}_s^T {\mathcal{L}^\dagger}^T \mathcal{L}^\dagger \mathcal{J}_s \right)^\dagger \mathcal{J}_s^T {\mathcal{L}^\dagger}^T \mathcal{L}^\dagger \mathcal{B}^T \zeta. \end{aligned}$$

Using the thin QR decomposition with column pivoting

$$\mathcal{L}^\dagger \mathcal{J}_s P = \mathcal{Q}\mathcal{R}, \tag{B4}$$

the test boils down to

$$\begin{aligned} t &= \zeta^T \mathcal{B}{\mathcal{L}^\dagger}^T \mathcal{Q}\mathcal{R} \left((\mathcal{Q}\mathcal{R})^T \mathcal{Q}\mathcal{R} \right)^\dagger (\mathcal{Q}\mathcal{R})^T \mathcal{L}^\dagger \mathcal{B}^T \zeta \\ &= \zeta^T \mathcal{B}{\mathcal{L}^\dagger}^T \mathcal{Q}\mathcal{R} \left(\mathcal{R}^\dagger \mathcal{Q}^T \mathcal{Q} {\mathcal{R}^T}^\dagger \right) \mathcal{R}^T \mathcal{Q}^T \mathcal{L}^\dagger \mathcal{B}^T \zeta = a^T a \end{aligned} \tag{B5}$$

where $a = \tilde{\mathcal{Q}}^T \mathcal{L}^\dagger \mathcal{B}^T \zeta$ and $\tilde{\mathcal{Q}}$ corresponds to the first columns of $\mathcal{Q}$ that correspond to non-zero diagonal entries in $\mathcal{R}$.

References

1. Rytter A. *Vibrational based inspection of civil engineering structures*. PhD thesis. Aalborg University, Aalborg, Denmark; 1993.

2. Peeters B, Maeck J, Roeck GD. Vibration-based damage detection in civil engineering: excitation sources and temperature effects. *Smart Materials and Structures* 2001; 10(3): 518-527.

3. Oliveira G, Magalhães F, Cunha Á, Caetano E. Vibration-based damage detection in a wind turbine using 1 year of data. *Structural Control and Health Monitoring* 2018; 25(11): e2238.

4. Bhuyan MDH, Gautier G, Le Touz N, et al. Vibration-based damage localization with load vectors under temperature changes. *Structural Control and Health Monitoring* 2019; 26(11): e2439.

5. Worden K, Manson G, Fieller NRJ. Damage detection using outlier analysis. *Journal of Sound and Vibration* 2000; 229(3): 647 - 667.

6. Dervilis N, Antoniadou I, Barthorpe R, Cross E, Worden K. Robust methods for outlier detection and regression for SHM applications. *International Journal of Sustainable Materials and Structural Systems* 2016; 2(1/2).

7. Ulriksen MD, Tcherniak D, Damkilde L. Damage detection in an operating Vestas V27 wind turbine blade by use of outlier analysis. In: IEEE Workshop on Environmental, Energy and Structural Monitoring Systems; 2015.

8. de Almeida Cardoso R, Cury A, Barbosa F, Gentile C. Unsupervised real-time SHM technique based on novelty indexes. *Structural Control and Health Monitoring* 2019: e2364.

9. Mahalanobis PC. On the generalised distance in statistics. In: Proceedings National Institute of Science, India; 1936: 49–55.

10. Balsamo L, Betti R. Data-based structural health monitoring using small training data sets. *Structural Control and Health Monitoring* 2015; 22(10): 1240–1264.

11. Zhou YL, Figueiredo E, Maia N, Sampaio R, Perera R. Damage detection in structures using a transmissibility-based Mahalanobis distance. *Structural Control and Health Monitoring* 2015; 22(10): 1209–1222.

12. Cross EJ, Worden K, Chen Q. Cointegration: a novel approach for the removal of environmental trends in structural health monitoring data. *Proceedings of the Royal Society A: Mathematical, Physical and Engineering Sciences* 2011; 467(2133): 2712-2732.

13. Shi H, Worden K, Cross EJ. A cointegration approach for heteroscedastic data based on a time series decomposition: An application to structural health monitoring. *Mechanical Systems and Signal Processing* 2019; 120: 16 - 31.

14. Bernal D. Kalman filter damage detection in the presence of changing process and measurement noise. *Mechanical Systems and Signal Processing* 2013; 39(1): 361 - 371.

15. Fugate ML, Sohn H, Farrar CR. Unsupervised learning methods for vibration-based damage detection. In: Proc. 18th International Modal Analysis Conference; 2000; San Antonio, Texas, USA.

16. Döhler M, Mevel L, Zhang Q. Fault detection, isolation and quantification from Gaussian residuals with application to structural damage diagnosis. *Annual Reviews in Control* 2016; 42: 244-256.

17. Chaabane M, Mansouri M, Ben Hamida A, Nounou H, Nounou M. Multivariate statistical process control-based hypothesis testing for damage detection in structural health monitoring systems. *Structural Control and Health Monitoring* 2019; 26(1): e2287.

18. Lei Y, Xia D, Erazo K, Nagarajaiah S. A novel unscented Kalman filter for recursive state-input-system identification of nonlinear systems. *Mechanical Systems and Signal Processing* 2019; 127: 120 - 135.

19. He J, Zhang X, Dai N. An improved Kalman filter for joint estimation of structural states and unknown loadings. *Smart Structures and Systems* 2019; 24(2): 209–221.

20. Ulriksen MD, Tcherniak D, Kirkegaard PH, Damkilde L. Operational modal analysis and wavelet transformation for damage identification in wind turbine blades. *Structural Health Monitoring* 2016; 15(4): 381-388.

21. Cha YJ, Wang Z. Unsupervised novelty detection-based structural damage localization using a density peaks-based fast clustering algorithm. *Structural Health Monitoring* 2018; 17(2): 313-324.

22. Zhu D, Yi X, Wang Y. A local excitation and measurement approach for decentralized damage detection using transmissibility functions. *Structural Control and Health Monitoring* 2016; 23(3): 487–502.

23. Yan WJ, Zhao MY, Sun Q, Ren WX. Transmissibility-based system identification for structural health monitoring: Fundamentals, approaches, and applications. *Mechanical Systems and Signal Processing* 2019; 117: 453 - 482.

24. Avci O, Abdeljaber O. Self-organizing maps for structural damage detection: a novel unsupervised vibration-based algorithm. *Journal of Performance of Constructed Facilities* 2016; 30(3): 04015043.

25. Tang Z, Chen Z, Bao Y, Li H. Convolutional neural network-based data anomaly detection method using multiple information for structural health monitoring. *Structural Control and Health Monitoring* 2019; 26(1): e2296.

26. Lei Y, Zhang Y, Mi J, Liu W, Liu L. Detecting structural damage under unknown seismic excitation by deep convolutional neural network with wavelet-based transmissibility data. *Structural Health Monitoring* 2020: 1475921720923081.

27. Wang Z, Cha YJ. Unsupervised deep learning approach using a deep auto-encoder with a one-class support vector machine to detect damage. *Structural Health Monitoring* 2021; 20(1): 406-425.

28. Vamvoudakis-Stefanou K, Sakellariou J, Fassois S. Vibration-based damage detection for a population of nominally identical structures: unsupervised Multiple Model (MM) statistical time series type methods. *Mechanical Systems and Signal Processing* 2018; 111: 149–171.

29. Doebling SW, Farrar CR, Prime MB. A summary review of vibration-based damage identification methods. *The Shock and Vibration Digest* 1998; 30(2): 91-105.

30. Lieven NAJ, Ewins DJ, Farrar CR, Doebling SW, Nix DA. Vibration-based structural damage identification. *Philosophical Transactions of the Royal Society of London. Series A: Mathematical, Physical and Engineering Sciences* 2001; 359(1778): 131-149.

31. Carden EP, Fanning P. Vibration based condition monitoring: A review. *Structural Health Monitoring* 2004; 3(4): 355-377.

32. Bhuyan MDH, Döhler M, Lecieux Y, Mevel L, Schoefs F. Statistical damage localization with stochastic load vectors using multiple mode sets. *Structural Health Monitoring* 2017; 16(5): 518–535.

33. Basseville M, Nikiforov IV. *Detection of abrupt changes: theory and application*. Englewood Cliffs: Prentice Hall . 1993.

34. Basseville M, Abdelghani M, Benveniste A. Subspace-based fault detection algorithms for vibration monitoring. *Automatica* 2000; 36(1): 101 - 109.

35. Döhler M, Mevel L, Hille F. Subspace-based damage detection under changes in the ambient excitation statistics. *Mechanical Systems and Signal Processing* 2014; 45(1): 207 - 224.

36. Yan AM, Golinval JC. Null subspace-based damage detection of structures using vibration measurements. *Mechanical Systems and Signal Processing* 2006; 20(3): 611 - 626.

37. Döhler M, Hille F, Mevel L, Rücker W. Structural health monitoring with statistical methods during progressive damage test of S101 Bridge. *Engineering Structures* 2014; 69: 183 - 193.

38. Ventura C, Andersen P, Mevel L, Döhler M. Structural health monitoring of the Pitt River Bridge in British Columbia, Canada. In: Proc. 6th World Conference on Structural Control and Monitoring; 2014; Barcelona, Spain.

39. Benveniste A, Basseville M, Moustakides G. The asymptotic local approach to change detection and model validation. *IEEE Transactions on Automatic Control* 1987; 32(7): 583-592.

40. Döhler M, Hille F, Mevel L. Vibration-based monitoring of civil structures with subspace-based damage detection. In: Ottaviano E, Pelliccio A, Gattulli V. , eds. *Mechatronics for Cultural Heritage and Civil Engineering*Cham: Springer International Publishing. 2018 (pp. 307–326).

41. Chen Y, Wu Q, He X, Jia W, Hintz T. A modified Mahalanobis distance for human detection in out-door environments. In: Proc. First IEEE International Conference on Ubi-Media Computing; 2008: 243-248.

42. Torra V, Abowd J, Domingo-Ferrer J. Using Mahalanobis distance-based record linkage for disclosure risk assessment. In: International Conference on Privacy in Statistical Databases; 2006: 233-242.

43. Greś S, Andersen P, Johansen RJ, Ulriksen MD, Damkilde L. A comparison of damage detection methods applied to civil engineering structures. In: Proceedings of the 7th International Conference on Experimental Vibration Analysis for Civil Engineering Structures; 2018.

44. Döhler M, Mevel L. Modular subspace-based system identification from multi-setup measurements. *IEEE Transactions on Automatic Control* 2012; 57(11): 2951-2956.

45. Döhler M, Lam XB, Mevel L. Uncertainty quantification for modal parameters from stochastic subspace identification on multi-setup measurements. *Mechanical Systems and Signal Processing* 2013; 36: 562-581.

46. Juang JN. *Applied System Identification*. Englewood Cliffs, NJ, USA: Prentice Hall . 1994.

47. Peeters B, de Roeck G. Reference-based stochastic subspace identification for output-only modal analysis. *Mechanical Systems and Signal Processing* 1999; 13(6): 855 - 878.

48. van Overschee P, de Moor B. *Subspace Identification for Linear Systems*. Springer. 1st ed. 1996.

49. Hardin J, Rocke DM. The distribution of robust distances. *Journal of Computational and Graphical Statistics* 2005; 14(4): 928-946.

50. Allahdadian S, Döhler M, Ventura C, Mevel L. Towards robust statistical damage localization via model-based sensitivity clustering. *Mechanical Systems and Signal Processing* 2019; 134: 106341.

51. Balmès E, Basseville M, Mevel L, Nasser H, Zhou W. Statistical model-based damage localization: A combined subspace-based and substructuring approach. *Structural Control and Health Monitoring* 2008; 15(6): 857–875.

52. Mellinger P, Döhler M, Mevel L. Variance estimation of modal parameters from output-only and input/output subspace-based system identification. *Journal of Sound and Vibration* 2016; 379: 1 - 27.

53. Viefhues E, Döhler M, Hille F, Mevel L. Asymptotic analysis of subspace-based data-driven residual for fault detection with uncertain reference. In: 10th IFAC Symposium on Fault Detection, Supervision and Safety for Technical Processes; 2018.

54. Casella G, Berger RL. *Statistical Inference*. Pacific Grove, CA, USA: Duxbury Press. 2nd ed. 2001.

55. Liu J, Liu X, Ma X. First-order perturbation analysis of singular vectors in singular value decomposition. *IEEE Transactions on Signal Processing* 2008; 56(7): 3044–3049.

56. Houlsby GT, Byrne BW. Suction caisson foundations for offshore wind turbines and anemometer masts. *Wind Engineering* 2000; 24(4): 249-255.

57. Houlsby G, Ibsen LB, Byrne B. Suction caissons for wind turbines. In: Proc. First International Symposium on Frontiers in Offshore Geotechnics; 2005.

58. Greś S, Ulriksen MD, Döhler M, et al. Statistical methods for damage detection applied to civil structures. *Procedia Engineering* 2017; 199: 1919 - 1924. X International Conference on Structural Dynamics, EURODYN 2017.

59. Greś S, Fejerskov M, Ibsen L, Damkilde L. Experimental damping assessment of a full scale offshore mono bucket foundation. In: Sas P, Moens D, van de Walle A. , eds. *Proceedings of ISMA2016*KU Leuven, Department of Mechanical Engineering, PMA; 2016: 4045–4054. The International Conference on Noise and Vibration Engineering, ISMA.

60. Greś S, Döhler M, Andersen P, Mevel L. Uncertainty quantification for the Modal Phase Collinearity of complex mode shapes. *Mechanical Systems and Signal Processing* 2021; 152: 107436.

61. Det-Norske-Veritas-GL . DNVGL-RP-0416. Corrosion Protection for Wind Turbines: Recommended Practice. *Offshore Standard* 2016.